Int J Adv Manuf Technol (2017) 90:1547–1568
DOI 10.1007/s00170-016-9467-6

ORIGINAL ARTICLE

Modeling of chip–tool interface temperature using response surface methodology and artificial neural network in HPC-assisted turning and tool life investigation

M. Kamruzzaman[1] · Saadman Sakib Rahman[2] · Md. Zurais Ibne Ashraf[2] · Nikhil Ranjan Dhar[3]

Received: 10 June 2016 / Accepted: 8 September 2016 / Published online: 27 September 2016

Abstract This study focuses on chip–tool interface temperature modeling of C-60, 17CrNiMo4, and 42CrMo4 steel alloys in dry-cut and high-pressure coolant (HPC)-assisted turning at various cutting speed-feed rates with SNMG and SNMM inserts. Improvement of tool life in turning C-60 steel under the application of jet at elevated pressure over dry machining is investigated. Scanning electron microscope (SEM) views of principal and auxiliary flank worn out tip (48-min) of cutting inserts divulge the effectiveness of high-pressure coolant emulsion over dry and conventional wet cooling. The experimental runs were conducted in full factorial orientation and response surface methodology (RSM) has been employed for subsequent modeling to formulate mathematical equations to devise accurate predictions of chip–tool interface temperature. Analysis of variance (ANOVA) is conducted to perceive the effects of each individual factors and their interactions terms and measure the significance of the proposed model. Later, optimization with desirability function concluded factor settings (cutting speed = 93 m/min, feed rate = 0.10 mm/rev, environment = HPC, material = C-60, and insert = SNMM) that minimize the response within the experimental domain satisfying desired goals. Further, artificial neural network (ANN) model has been developed and the prediction performance was compared with the cubic equations of RSM. It was observed that during testing phase MAPE and coefficient of determination (R^2) for RSM is 1.947 and 94.48 %, respectively; and the corresponding values for ANN (4-22-1) is 2.669 and 93.25 %. Results also reveal that cutting speed and environment have ~38.82 and ~37.82 % contribution on chip–tool interface temperature formation during machining. In addition, the results showed that HPC-assisted machining reduces chip–tool interface temperature significantly as well as prolong tool life.

Keywords Chip–tool interface temperature · HPC-assisted machining · Scanning electron microscope · Response surface methodology · Analysis of variance · Artificial neural network

1 Introduction

Machining is a manufacturing process where a sharp cutting tool penetrates the surface of a less-resistant work material due to the relative motion of the tool and the workpiece and cutting forces exerted by cutting insert at the tool–work contact zone. The penetration causes shear deformation of the workpiece in order to remove material from the surface in the form of chips. During the formation of chips, the mechanical energy applied by the insert converts to heat energy. In case of ductile materials, the heat is generated at three distinguish zones: (a) primary deformation zone, (b) chip–tool interface, and (c) work–tool interface zones which adversely influence the quality of the finished product as well as the cutting insert [1]. Plastic deformation of the work material, rubbing of the tool flank with the finished surface and friction between tool rake face, and flowing chips foster intense amount of heat at the cutting zone [2]. Furthermore, heat is also generated by the friction at

✉ Saadman Sakib Rahman
saad_ie@outlook.com

[1] Mechanical Engineering, Dhaka University of Engineering and Technology, Gazipur, Bangladesh

[2] Mechanical and Production Engineering, Ahsanullah University of Science and Technology, Dhaka 1208, Bangladesh

[3] Industrial and Production Engineering, Bangladesh University of Engineering and Technology, Dhaka 1000, Bangladesh

the work and tool tip contact zone [3]. This frictional heat is one of the major causes of reduction in tool hardness and rapid tool wear which must be controlled by the application of cutting fluids or coolants in the form of liquid or gas directed at the hot cutting region. However, traditional methods of heat extraction with the use of conventional coolants become less effective during high productivity machining at augmented feed rate and cutting speed as smooth flow to the chip–tool interface often gets prevented due to bulk plastic contact of the chip with the tool rake surface [4, 5]. Moreover, the use of conventional coolant exhibits some other drawbacks such as, it does not reach the tool–workpiece and chip–tool interfaces where the maximum temperature attains [6] as sometimes extensive heat evaporates the coolant before it can reach the cutting region and creates a semi-conductive high-temperature blanket which renders the cooling effect to a great extent, also the usage of coolant causes serious damage to human health and environment [7]. In many cases, the uses of coolants are still essential to attain economic feasibility by achieving improved tool life and ameliorated surface quality. Cryogenic machining [8, 9], minimum quantity lubrication (MQL) [10], near dry machining [11], high-pressure coolant jet [12], and ultra-high-pressure coolant jet [13] are the recent developments in manufacturing research sector and industrial applications.

Despite the increased usage and production of C-60 steel, they have relatively poor machinability characteristics compared to many other metals, because of the complexity of the heat extraction process. 17CrNiMo4 steel is mainly used for heavy-duty arbors, bushings, wear pins, bearings, sprockets, gears, shafts, and other high-tensile applications. 42CrMo4 is a common chromium-molybdenum alloy steel with high hardenability and good toughness. The carbon content of 42CrMo4 steel alloy is very high and mainly used in automobile industries to make gears and in the manufacture of forgings which require higher strength. Such materials are very difficult to machine and intense amount of heat generates during machining which must be reduced to ameliorate product quality and dimensional accuracy by proper application of coolant and/or lubricant. Again, because of high hardness of these materials, huge amount of friction generates at the tool tip. As a result, the tool wears more rapidly causing significant decrease in tool life. For such applications, high-pressure coolant (HPC)-assisted machining is the preferred technology. For instance, a comparative analysis has been conducted by M. Bermingham et al. [14] between cryogenic cooling and high-pressure emulsion cooling techniques in Ti-6Al-4V turning, where tool life and chip morphology have been considered as the quality characteristics. It has been observed that high-pressure emulsion offers slightly better tool life than that achievable with liquid nitrogen coolant. According to E. O. Ezugwu [15], HPC-assisted machining forms a hydraulic wedge between the tool and workpiece due to the application of jet, under elevated pressure. Penetration of the jet equipped with high velocity and energy reduces temperature gradient and seizure zone [16] also known as a very thin flow zone along the greater part of the contact between the chip and the tool, where the two materials associated are in intimate contact and no relative movement between the chip and the tool at the surface of the tool. This offers an adequate lubrication at the chip–tool interface with a significant reduction in friction [17]. Braham-Bouchnak T et al. [18] studied the effects of high-pressure coolant assisted turning of the Ti555-3 titanium alloy. It has been reported that good chip fragmentation and significant improvement of tool life and surface integrity are achieved during HPC-assisted machining. Naves V et al. [19] investigated the wear mechanism of coated cemented carbide tools during turning operation of AISI 316 stainless steel. Cutting fluid was applied at various pressures (10, 15, and 20 MPa) between the chip and tool at the rake face. They observed that the lowest flank wear-land was obtained when the concentration of the cutting fluid was 10 % and pressure was 10 MPa; the application of HPC jet is recommended over dry machining during turning of the investigated stainless steel.

Response surface methodology (RSM) is embraced by many researchers to develop an effective empirical relationship between dependent responses and independent process parameters to measure the effects of various machining factors on the performance characteristics such as surface roughness [20, 21], cutting force [21, 22], tool wear [23], cutting temperature [24, 25], and other machining quality characteristics. Further, response surface equations have been used to make accurate predictions of one or more responses efficiently prior to machining, i.e., turning, hard turning, milling, drilling, and also grinding. Abhang L et al. [26] used the response surface methodology for modeling chip–tool interface temperature measured in turning of EN-31 steel alloy with tungsten carbide inserts. In their experimental research work, first- and second-order mathematical models were established to show the relationship between the response and metal cutting parameters associated with the response such as cutting speed, feed rate, depth of cut, and nose radius. *R*-squared values for the first- and second-order models were found to be 97.68 and 98.90 %, respectively. Additionally, analysis of variance (ANOVA) results revealed that cutting speed has the most dominant effect on determining chip–tool interface temperature. Sharma MD et al. [27] developed mathematical models to evaluate the effects of cutting speed, feed rate, and depth of cut on main cutting force, surface roughness, and stress where average errors of 3.87, 5.41, and 2.96 % were observed individually. Çalışkan H et al. [28] investigated the influence of hard coatings and cutting parameters such as cutting speed, feed rate, and depth of cut on cutting forces and surface roughness during face milling of AISI O2 cold work–tool steel-based on response surface methodology. The response surface equations exhibited high coefficient of determination which

Table 1 Experimental conditions

Machine tool	Centre Lathe (10 HP), China
Work materials	•C-60 steel (Size: Ø178 × 580 mm, BHN: 195)
	•17CrNiMo6 steel (Size: Ø200 × 520 mm, BHN: 201)
	•42CrMo4 steel (Size: Ø220 × 520 mm, BHN: 252)
Cutting insert	SNMG and SNMM 120408 TTS, Sandvik (ISO Specification)
Tool holder	PSBNR 2525M12, Sandvik
Working tool geometry	−6°, −6°, 6°, 6°, 15°, 75°, 0.8 mm
Process parameters	
Cutting speed, V	93,133, 186, 266 m/min
	133, 152, and 186 m/min (for tool life investigation)
Feed rate, f	0.10, 0.14, 0.18 and 0.22 mm/rev
	0.14, 0.18, and 0.22 mm/rev (for tool life investigation)
Depth of cut, d	1.0 mm
	1.5 mm (for tool life investigation)
High-pressure coolant (HPC)	80 bar, Coolant: 6.0 l/min through external nozzle
Coolant type	VG-68 (ISO grade)
Environments	•Dry
	•Wet (only for C-60)
	•High-pressure coolant (HPC) condition

proves the adequacy of the method applied. Amini et al. [29] used regression analysis to investigate the effects possessed by cutting speed, feed rate, and depth of cut on surface roughness and cutting force in high-speed turning of Inconel 718 with ceramic and carbide cutting tools. Literature suggests that even though lots of studies have been performed employing response surface methodology during turning of different alloys and steels but most of them are concerned with mainly surface roughness and cutting forces. As controlling cutting temperature is one the most challenging factor during turning of any material, so it is necessary to study the effect possessed by various machining parameters, different machining environments, materials, and cutting inserts. Reliable mathematical models must be formulated to efficiently and accurately predict the value prior to machining which will not only reduce the product cost but also will diminish unnecessary power consumption and machining time to aid the manufacturers and industry practitioners.

Artificial intelligence-based models such as artificial neural network is efficient, easy to operate, and more accurate than many existing models to make predictions even if it has to deal with noisy or vast amount of data. Recently, it gained much

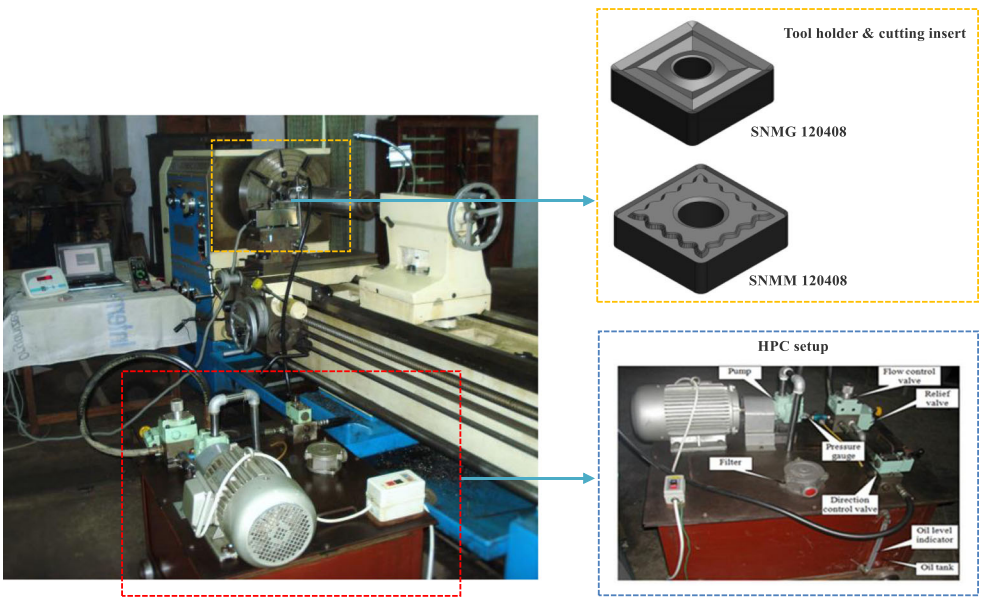

Fig. 1 Experimental set-up

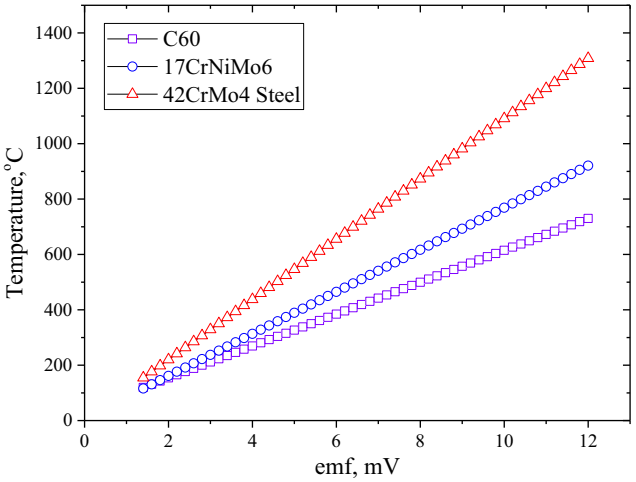

Fig. 2 Tool–work thermocouple calibration curve

appreciation among the researchers and manufacturers. T. Özel et al. [30] developed feedforward back propagation neural network models to predict surface roughness and tool flank wear in finish dry hard turning and also compared the prediction accuracy of the developed models with regression models. It was anticipated that neural networks are well capable to predict surface roughness and tool wear accurately and provided better performance than regression model. K.V. Rao et al. [31] used a multilayer perceptron artificial neural network (ANN) model (4-14-8-3) where cutting speed, feed rate, nose radius, and volume of metal are given as input and surface roughness, tool wear, and workpiece amplitude were the responses. It was reported that the developed neural network model can be used to select proper cutting parameters to reduce surface roughness, tool wear, and tool vibration during boring of AISI 316 steel. R. Kumar et al. [32] studied the effects of cutting speed, feed rate, and approach angle on surface finish during turning of Al 7075 hard ceramic composite and Al 7075 hybrid composite, using PCD cutting tool. RSM and ANN techniques were applied to predict the response where ANN model produced more percentage error compared to RSM modeling. Artificial neural network is also being used by some researchers to predict cutting temperature at the chip–tool interface [33–35]. Neural network model to predict cutting temperature during orthogonal machining of AISI 316L stainless steel was developed by F. Kara et al. [36]. After evaluating the performance, it was suggested that the learning capability of the neural network model is quite powerful and highly recommended for prediction of cutting temperatures without conducting the complicated, expensive, and time-consuming experimental studies. Absolute mean error percentage (MEP) for the predicted values was within ± 5 % error limits. Korkut I et al. [37] developed regression and artificial neural network models to predict tool–chip interface temperature. The results revealed that both RA and ANN model are capable to make accurate predictions of the response of interest but ANN showed better performance.

Many researchers studied about the implementation and performance of neural networks on machining where the performance is measured in terms of numerical inputs to the networks without considering categorical inputs or mixture of both. In modern day machining, manufacturers are not only concerned about selecting the most efficient set of machining parameters in terms of feed rate, cutting speed, depth of cut, nose radius, cutting force, etc. but also have to test and adopt various materials, different cutting fluid applications, cutting inserts, etc. in order to achieve their desired goals and high precision of results. The literatures also indicate that there is no sufficient amount of neural network modeling available regarding prediction of chip–tool interface cutting temperature prior to machining. According to authors' knowledge, no research has been conducted yet to show the performance of ANN in chip–tool interface temperature prediction capability under high-pressure coolant application and straight turning of C-60, 17CrNiMo6, and 42CrMo4 steel rods with SNMG and SNMM inserts; and aforesaid categorical factors are used in network development as input to the network along with various speed-feed combinations.

In the present study, the role of high-pressure coolant jet by water-insoluble mineral oil VG-68 on cutting temperature and tool life in turning C-60 steel, 17CrNiMo6 steel, and 42CrMo4 steel by uncoated SNMG and SNMM carbide inserts is experimentally investigated. To evaluate the effects of cutting speed, feed rate, environment (dry and HPC-assisted machining), materials, and cutting inserts on chip–tool interface temperature, mathematical models are formed based on response surface methodology and validity of the models are confirmed by employing various statistical evaluation techniques. Further, artificial neural network model has been established to make accurate predictions of chip–tool interface temperature which is later compared with the response surface

Table 2 Factors along with their values and levels

Factor	Name	Units	Type	Level 1	Level 2	Level 3	Level 4
A	Cutting speed	m/min	Numeric	93	133	186	266
B	Feed rate	mm/rev	Numeric	0.10	0.14	0.18	0.22
C	Environment		Categorical	Dry	HPC	–	–
D	Material		Categorical	C-60	17CrNiMo6	42CrMo4	–
E	Cutting tool		Categorical	SNMG	SNMM	–	–

Table 3 Response surface methodology (full factorial) design layout

Run	Cutting speed	Feed rate	Env.	Material	Insert	Response
84	93	0.1	Dry	C-60	SNMG	592
73	93	0.14	Dry	C-60	SNMG	662
53	93	0.18	Dry	C-60	SNMG	694
70	93	0.22	Dry	C-60	SNMG	698
25	133	0.1	Dry	C-60	SNMG	652
81	133	0.14	Dry	C-60	SNMG	694
87	133	0.18	Dry	C-60	SNMG	709
1	133	0.22	Dry	C-60	SNMG	736
4	186	0.1	Dry	C-60	SNMG	714
114	186	0.14	Dry	C-60	SNMG	769
98	186	0.18	Dry	C-60	SNMG	782
40	186	0.22	Dry	C-60	SNMG	790
142	266	0.1	Dry	C-60	SNMG	773
164	266	0.14	Dry	C-60	SNMG	821
104	266	0.18	Dry	C-60	SNMG	826
54	266	0.22	Dry	C-60	SNMG	843
60	93	0.1	HPC	C-60	SNMG	453
23	93	0.14	HPC	C-60	SNMG	534
124	93	0.18	HPC	C-60	SNMG	563
17	93	0.22	HPC	C-60	SNMG	584
43	133	0.1	HPC	C-60	SNMG	566
59	133	0.14	HPC	C-60	SNMG	595
83	133	0.18	HPC	C-60	SNMG	617
157	133	0.22	HPC	C-60	SNMG	640
5	186	0.1	HPC	C-60	SNMG	595
135	186	0.14	HPC	C-60	SNMG	644
13	186	0.18	HPC	C-60	SNMG	678
12	186	0.22	HPC	C-60	SNMG	701
74	266	0.1	HPC	C-60	SNMG	697
118	266	0.14	HPC	C-60	SNMG	717
6	266	0.18	HPC	C-60	SNMG	757
123	266	0.22	HPC	C-60	SNMG	784
16	93	0.1	Dry	17CrNiMo6	SNMG	690
86	93	0.14	Dry	17CrNiMo6	SNMG	564
90	93	0.18	Dry	17CrNiMo6	SNMG	708
131	93	0.22	Dry	17CrNiMo6	SNMG	591
186	133	0.1	Dry	17CrNiMo6	SNMG	730
113	133	0.14	Dry	17CrNiMo6	SNMG	646
122	133	0.18	Dry	17CrNiMo6	SNMG	743
191	133	0.22	Dry	17CrNiMo6	SNMG	671
127	186	0.1	Dry	17CrNiMo6	SNMG	780
65	186	0.14	Dry	17CrNiMo6	SNMG	706
183	186	0.18	Dry	17CrNiMo6	SNMG	791
165	186	0.22	Dry	17CrNiMo6	SNMG	724
19	266	0.1	Dry	17CrNiMo6	SNMG	826
162	266	0.14	Dry	17CrNiMo6	SNMG	757
125	266	0.18	Dry	17CrNiMo6	SNMG	839
106	266	0.22	Dry	17CrNiMo6	SNMG	770
133	93	0.1	HPC	17CrNiMo6	SNMG	566
126	93	0.14	HPC	17CrNiMo6	SNMG	468
100	93	0.18	HPC	17CrNiMo6	SNMG	581
160	93	0.22	HPC	17CrNiMo6	SNMG	491
128	133	0.1	HPC	17CrNiMo6	SNMG	606
120	133	0.14	HPC	17CrNiMo6	SNMG	549
166	133	0.18	HPC	17CrNiMo6	SNMG	624
109	133	0.22	HPC	17CrNiMo6	SNMG	590
64	186	0.1	HPC	17CrNiMo6	SNMG	679
37	186	0.14	HPC	17CrNiMo6	SNMG	628
29	186	0.18	HPC	17CrNiMo6	SNMG	680
94	186	0.22	HPC	17CrNiMo6	SNMG	644
11	266	0.1	HPC	17CrNiMo6	SNMG	710
76	266	0.14	HPC	17CrNiMo6	SNMG	651
97	266	0.18	HPC	17CrNiMo6	SNMG	738
107	266	0.22	HPC	17CrNiMo6	SNMG	701
139	93	0.1	Dry	42CrMo4	SNMG	671
190	93	0.14	Dry	42CrMo4	SNMG	688
79	93	0.18	Dry	42CrMo4	SNMG	707
177	93	0.22	Dry	42CrMo4	SNMG	713
49	133	0.1	Dry	42CrMo4	SNMG	692
101	133	0.14	Dry	42CrMo4	SNMG	732
172	133	0.18	Dry	42CrMo4	SNMG	736
52	133	0.22	Dry	42CrMo4	SNMG	749
75	186	0.1	Dry	42CrMo4	SNMG	712
168	186	0.14	Dry	42CrMo4	SNMG	746
181	186	0.18	Dry	42CrMo4	SNMG	767
140	186	0.22	Dry	42CrMo4	SNMG	786
119	266	0.1	Dry	42CrMo4	SNMG	739
20	266	0.14	Dry	42CrMo4	SNMG	769
134	266	0.18	Dry	42CrMo4	SNMG	799
95	266	0.22	Dry	42CrMo4	SNMG	823
182	93	0.1	HPC	42CrMo4	SNMG	510
69	93	0.14	HPC	42CrMo4	SNMG	523
68	93	0.18	HPC	42CrMo4	SNMG	573
14	93	0.22	HPC	42CrMo4	SNMG	613
51	133	0.1	HPC	42CrMo4	SNMG	547
78	133	0.14	HPC	42CrMo4	SNMG	586
148	133	0.18	HPC	42CrMo4	SNMG	633
31	133	0.22	HPC	42CrMo4	SNMG	667
155	186	0.1	HPC	42CrMo4	SNMG	577
39	186	0.14	HPC	42CrMo4	SNMG	619
47	186	0.18	HPC	42CrMo4	SNMG	667
176	186	0.22	HPC	42CrMo4	SNMG	715
48	266	0.1	HPC	42CrMo4	SNMG	621
137	266	0.14	HPC	42CrMo4	SNMG	669
44	266	0.18	HPC	42CrMo4	SNMG	727
112	266	0.22	HPC	42CrMo4	SNMG	757
167	93	0.1	Dry	C-60	SNMM	565

Table 3 (continued)

Run	Cutting speed	Feed rate	Env.	Material	Insert	Response
111	93	0.14	Dry	C-60	SNMM	641
36	93	0.18	Dry	C-60	SNMM	682
92	93	0.22	Dry	C-60	SNMM	691
7	133	0.1	Dry	C-60	SNMM	618
188	133	0.14	Dry	C-60	SNMM	670
149	133	0.18	Dry	C-60	SNMM	697
117	133	0.22	Dry	C-60	SNMM	713
45	186	0.1	Dry	C-60	SNMM	680
50	186	0.14	Dry	C-60	SNMM	744
192	186	0.18	Dry	C-60	SNMM	757
56	186	0.22	Dry	C-60	SNMM	790
102	266	0.1	Dry	C-60	SNMM	727
136	266	0.14	Dry	C-60	SNMM	788
63	266	0.18	Dry	C-60	SNMM	813
15	266	0.22	Dry	C-60	SNMM	822
99	93	0.1	HPC	C-60	SNMM	470
175	93	0.14	HPC	C-60	SNMM	540
170	93	0.18	HPC	C-60	SNMM	566
41	93	0.22	HPC	C-60	SNMM	578
27	133	0.1	HPC	C-60	SNMM	526
32	133	0.14	HPC	C-60	SNMM	568
67	133	0.18	HPC	C-60	SNMM	587
173	133	0.22	HPC	C-60	SNMM	634
55	186	0.1	HPC	C-60	SNMM	582
88	186	0.14	HPC	C-60	SNMM	638
163	186	0.18	HPC	C-60	SNMM	681
178	186	0.22	HPC	C-60	SNMM	703
116	266	0.1	HPC	C-60	SNMM	631
8	266	0.14	HPC	C-60	SNMM	697
103	266	0.18	HPC	C-60	SNMM	711
62	266	0.22	HPC	C-60	SNMM	755
189	93	0.1	Dry	17CrNiMo6	SNMM	645
61	93	0.14	Dry	17CrNiMo6	SNMM	672
33	93	0.18	Dry	17CrNiMo6	SNMM	709
180	93	0.22	Dry	17CrNiMo6	SNMM	728
72	133	0.1	Dry	17CrNiMo6	SNMM	707
158	133	0.14	Dry	17CrNiMo6	SNMM	741
143	133	0.18	Dry	17CrNiMo6	SNMM	760
96	133	0.22	Dry	17CrNiMo6	SNMM	777
21	186	0.1	Dry	17CrNiMo6	SNMM	771
26	186	0.14	Dry	17CrNiMo6	SNMM	803
93	186	0.18	Dry	17CrNiMo6	SNMM	812
141	186	0.22	Dry	17CrNiMo6	SNMM	826
9	266	0.1	Dry	17CrNiMo6	SNMM	823
3	266	0.14	Dry	17CrNiMo6	SNMM	846
121	266	0.18	Dry	17CrNiMo6	SNMM	858
169	266	0.22	Dry	17CrNiMo6	SNMM	865
132	93	0.1	HPC	17CrNiMo6	SNMM	522
24	93	0.14	HPC	17CrNiMo6	SNMM	551

Table 3 (continued)

Run	Cutting speed	Feed rate	Env.	Material	Insert	Response
187	93	0.18	HPC	17CrNiMo6	SNMM	588
147	93	0.22	HPC	17CrNiMo6	SNMM	612
18	133	0.1	HPC	17CrNiMo6	SNMM	573
2	133	0.14	HPC	17CrNiMo6	SNMM	600
66	133	0.18	HPC	17CrNiMo6	SNMM	638
38	133	0.22	HPC	17CrNiMo6	SNMM	660
57	186	0.1	HPC	17CrNiMo6	SNMM	655
28	186	0.14	HPC	17CrNiMo6	SNMM	675
129	186	0.18	HPC	17CrNiMo6	SNMM	690
150	186	0.22	HPC	17CrNiMo6	SNMM	743
82	266	0.1	HPC	17CrNiMo6	SNMM	691
159	266	0.14	HPC	17CrNiMo6	SNMM	728
35	266	0.18	HPC	17CrNiMo6	SNMM	746
184	266	0.22	HPC	17CrNiMo6	SNMM	770
30	93	0.1	Dry	42CrMo4	SNMM	673
91	93	0.14	Dry	42CrMo4	SNMM	686
151	93	0.18	Dry	42CrMo4	SNMM	700
108	93	0.22	Dry	42CrMo4	SNMM	713
161	133	0.1	Dry	42CrMo4	SNMM	703
179	133	0.14	Dry	42CrMo4	SNMM	720
42	133	0.18	Dry	42CrMo4	SNMM	735
85	133	0.22	Dry	42CrMo4	SNMM	745
89	186	0.1	Dry	42CrMo4	SNMM	736
77	186	0.14	Dry	42CrMo4	SNMM	746
22	186	0.18	Dry	42CrMo4	SNMM	753
34	186	0.22	Dry	42CrMo4	SNMM	771
71	266	0.1	Dry	42CrMo4	SNMM	764
138	266	0.14	Dry	42CrMo4	SNMM	780
130	266	0.18	Dry	42CrMo4	SNMM	797
145	266	0.22	Dry	42CrMo4	SNMM	811
115	93	0.1	HPC	42CrMo4	SNMM	505
156	93	0.14	HPC	42CrMo4	SNMM	528
105	93	0.18	HPC	42CrMo4	SNMM	560
171	93	0.22	HPC	42CrMo4	SNMM	606
185	133	0.1	HPC	42CrMo4	SNMM	534
144	133	0.14	HPC	42CrMo4	SNMM	576
174	133	0.18	HPC	42CrMo4	SNMM	595
154	133	0.22	HPC	42CrMo4	SNMM	671
110	186	0.1	HPC	42CrMo4	SNMM	581
153	186	0.14	HPC	42CrMo4	SNMM	612
146	186	0.18	HPC	42CrMo4	SNMM	663
10	186	0.22	HPC	42CrMo4	SNMM	694
58	266	0.1	HPC	42CrMo4	SNMM	634
152	266	0.14	HPC	42CrMo4	SNMM	654
46	266	0.18	HPC	42CrMo4	SNMM	733
80	266	0.22	HPC	42CrMo4	SNMM	754

Table 4 Design summary of the response

Response	Name	Unit	Obs.	Min.	Max.	Mean	Std. Dev.	Ratio	Model
R1	Chip–tool interface temperature	°C	192	453	865	681.969	88.7455	1.90949	Cubic

mathematical prediction model. The effects of cutting speed, feed rate, environment, and tool inserts on tool life are also measured by performing ANOVA. The scanning electron microscope (SEM) views of inserts under dry, wet, and HPC environment during turning of C-60 steel are compared to each other to evaluate the performance of HPC jet on tool wear reduction rate. It is expected that HPC-assisted machining will reduce chip–tool interface temperature and improve tool life significantly during turning operation of the selected materials. The outcomes of this research study are expected to aid the manufacturers and industrial practitioners to, effectively and efficiently, control and adopt the HPC-assisted machining process, promote higher productivity, and know about the result prior to actual machining. Furthermore, it will help the researchers to implement these techniques to model other machining processes and accelerate the pace by researches.

2 Experimental conditions and set-up

Straight turning of C-60, 17CrNiMo6, and 42CrMo4 steel rod of common use in a rigid and reasonably powerful lathe (10 HP, China) have been carried out by standard carbide inserts (SNMG and SNMM, Sandvik) at discrete cutting speeds and feed rates under both dry and high-pressure coolant (HPC) machining conditions. The detailed experimental conditions are stated in Table 1. The ranges of the cutting speed and feed rate were selected based on the tool manufacturer's recommendation and industrial practices. Depth of cut is less significant as it only changes the magnitude of cutting forces and was kept constant to 1.0 mm all through the experimental domain of investigating cutting temperature. However, depth of cut was kept at 1.5 mm during the investigation of tool life. Tool inserts were replaced after each cut so that the results are not affected due to wear. The experimental set-up used for the present purpose is shown in Fig. 1.

An important part of the HPC system is the design of a nozzle. The purpose of a nozzle is to direct cutting fluid to the optimal position to achieve maximum fluid flow at the chip–tool interface. It also fulfills the purpose of increasing the fluid velocity by contracting the cross-sectional area of the jet stream. High-pressure coolant jet was impinged from a specially designed nozzle to cool the tool and the work material at the hot cutting zone. The thin but high velocity stream of coolant was projected along the auxiliary cutting edge of the insert making an angle 15° with true horizontal. The nozzle was placed 15 mm away from the tool tip to minimize the interference of the nozzle with the flowing chips and to reach quite close to the chip–tool contact zone without avoiding of bulk cooling of the tool and the job, which may cause unfavorable metallurgical changes. Considering the jet pattern and to cover the entire cutting area by issuing jet, the nozzle bore diameter was selected as 0.5 mm. Pump pressurizes the coolant at a pressure of 80 bars with a flow rate of 6 l/min. Effectiveness of cooling depends on how closely HPC jet can reach the chip–tool and the work–tool interfaces, where apart from shear zone, heat is generated. The tool geometry is reasonably expected to play significant role on such cooling effectiveness. For the present investigations, two different tools namely SNMG 120408-TTS and SNMM 120408-TTS have been undertaken. Standard Sandvik PSBNR 2525M12 tool holder was used to hold the inserts.

The average chip–tool interface temperature was measured under all the machining conditions undertaken by reliable tool–work thermocouple technique with proper calibration [12]. In the present study, almost linear relationships between the temperature and electromotive force (emf) is obtained with multiple correlation coefficients around 0.994. Tool–work thermocouple calibration curves are shown in Fig. 2. According to ISO 3685 Standard (the International Organization for Standardization) specification of finish operation, tool was rejected when the growth of the average wear on its principle flank reached to 300-μm limit or maximum flank wear exceeded 600 μm. When the tool operation reached its 48-min mark, it was inspected under scanning electron microscope (Philips XL30) to study the wear mechanism and for the purpose of comparison.

Table 5 Statistics of the models

Source	*P* value	*R*-squared (adjusted)	*R*-squared (predicted)	
Linear	<0.0001	0.8598	0.8531	
2FI	<0.0001	0.9216	0.9109	
Quadratic	<0.0001	0.9328	0.9228	
Cubic	<0.0001	0.9512	0.9366	Suggested
Quartic	<0.0001	0.9685	0.9432	Aliased

3 Experimental results and discussion

To improve cutting performance, a cutting fluid in the form of liquid or gas must be applied directly to the cutting zone [38]. Machining generates huge amounts of heat at the shear and frictional zones; such heat generation increases with the increase in process parameters due to high-energy input causing decrease in hardness of the contact layer of the workpiece and

Table 6 Analysis of variance table (classical sum of squares—Type II)

Source	Sum of squares	df	Mean square	*F* value	P value (Prob > F)	
Model	1.450E + 006	50	29,001.39	75.45	<0.0001	Significant
A-Cutting speed	5.839E + 005	1	5.839E + 005	1518.92	<0.0001	Significant
B-Feed rate	1.360E + 005	1	1.360E + 005	353.78	<0.0001	Significant
C-Environment	5.688E + 005	1	5.688E + 005	1479.62	<0.0001	Significant
D-Material	9296.28	2	4648.14	12.09	<0.0001	Significant
E-Cutting tool	2054.08	1	2054.08	5.34	0.0222	Significant
AB	25.15	1	25.15	0.065	0.7985	
AC	5999.41	1	5999.41	15.61	0.0001	Significant
AD	15,916.08	2	7958.04	20.70	<0.0001	Significant
AE	187.16	1	187.16	0.49	0.4865	
BC	8652.00	1	8652.00	22.51	<0.0001	Significant
BD	25,797.34	2	12,898.67	33.56	<0.0001	Significant
BE	6636.02	1	6636.02	17.26	<0.0001	Significant
CD	2837.70	2	1418.85	3.69	0.0274	Significant
CE	408.33	1	408.33	1.06	0.3045	
DE	32,193.95	2	16,096.97	41.88	<0.0001	Significant
A^2	15,015.01	1	15,015.01	39.06	<0.0001	Significant
B^2	1220.08	1	1220.08	3.17	0.0770	
ABC	334.58	1	334.58	0.87	0.3524	
ABD	1137.92	2	568.96	1.48	0.2311	
ABE	333.14	1	333.14	0.87	0.3535	
ACD	1490.82	2	745.41	1.94	0.1476	
ACE	147.55	1	147.55	0.38	0.5365	
ADE	1069.16	2	534.58	1.39	0.2523	
BCD	4249.81	2	2124.91	5.53	0.0049	Significant
BCE	2.02	1	2.02	5.246E-003	0.9424	
BDE	13,286.91	2	6643.46	17.28	<0.0001	Significant
CDE	1074.57	2	537.29	1.40	0.2506	
A^2B	4.68	1	4.68	0.012	0.9123	
A^2C	181.83	1	181.83	0.47	0.4927	
A^2D	2146.73	2	1073.37	2.79	0.0647	
A^2E	37.25	1	37.25	0.097	0.7560	
AB^2	13.45	1	13.45	0.035	0.8519	
B^2C	784.08	1	784.08	2.04	0.1554	
B^2D	3354.82	2	1677.41	4.36	0.0145	Significant
B^2E	42.19	1	42.19	0.11	0.7409	
A^3	60.53	1	60.53	0.16	0.6921	
B^3	5453.07	1	5453.07	14.19	0.0002	Significant
Residual	54,200.17	141	384.40			
Corrected Total	1.504E + 006	191				

also the tool material. High temperature at the cutting zone has detrimental effect on cutting tool as well as surface finish so it must be controlled to improve machinability index. Cutting fluid reduces not only the generation of heat at the shear and friction zone but also friction at the tool–chip and tool–work interfaces. Various forms of cutting fluids are commercially available each with unique characteristics, advantages, and disadvantages [39]. In this section, along with subsequent modeling, the effect of high-pressure coolant on average chip–tool interface temperature at different cutting speeds, feed rates, steels, and inserts has been investigated. A total of five factors are involved in this experiment. Among them, two numeric factors: cutting speed and feed rate and three categorical factors: environment, material, and cutting tool which are in the nominal form are shown in Table 2 with their specified levels. The response considered in this study is chip–tool interface temperature. According to RSM design layout, shown in Table 3, a total of 192 observations are made where maximum and minimum measured value of chip–tool temperature are 865 and 453 °C, respectively. The statistics of the observed response are stated in Table 4. Response surface design modeling was carried out in Design-Expert software, version 10. No transformation of the response was made as the ratio of the maximum to minimum value of the response is found to be 1.90949. Usually, a ratio greater than 10 indicates a transformation is required as well as for ratios less than 3 the power transformations have little effect.

3.1 Chip–tool interface temperature modeling by RSM

The regression calculations have been made to fit all of the polynomial models of chip–tool interface temperature. Statistics such as *P* value, adjusted *R*-squared and predicted *R*-squared values are shown in Table 5 to compare the models. Here, *P* value is the probability that the factors and their interaction terms used in this study are modeling noise rather than helping explain the trend in the chip–tool interface temperature observations. The amount of variation in the response that can be explained by the model is represented by the adjusted *R*-squared value. The predicted residual error sum of squares (PRESS) statistics [40] is a form of cross-validation used in regression analysis to provide a measure of how a particular model fits each design point. Predicted *R*-squared value is calculated from PRESS statistics which represents the amount of variation in data predicted by the model. Models that have larger predicted *R*-squared values have better capability to make accurate predictions. Evaluating the statistics of all the models, cubic model has been chosen for the study. For the selected model, the adjusted *R*-squared of 0.9512 is in reasonable agreement with the predicted *R*-squared of 0.93266. The difference between them is within approximately 0.02 which indicates the significance of the developed model. Quartic and higher models are aliased, which means not enough experiments have been run to independently estimate all the terms for this model.

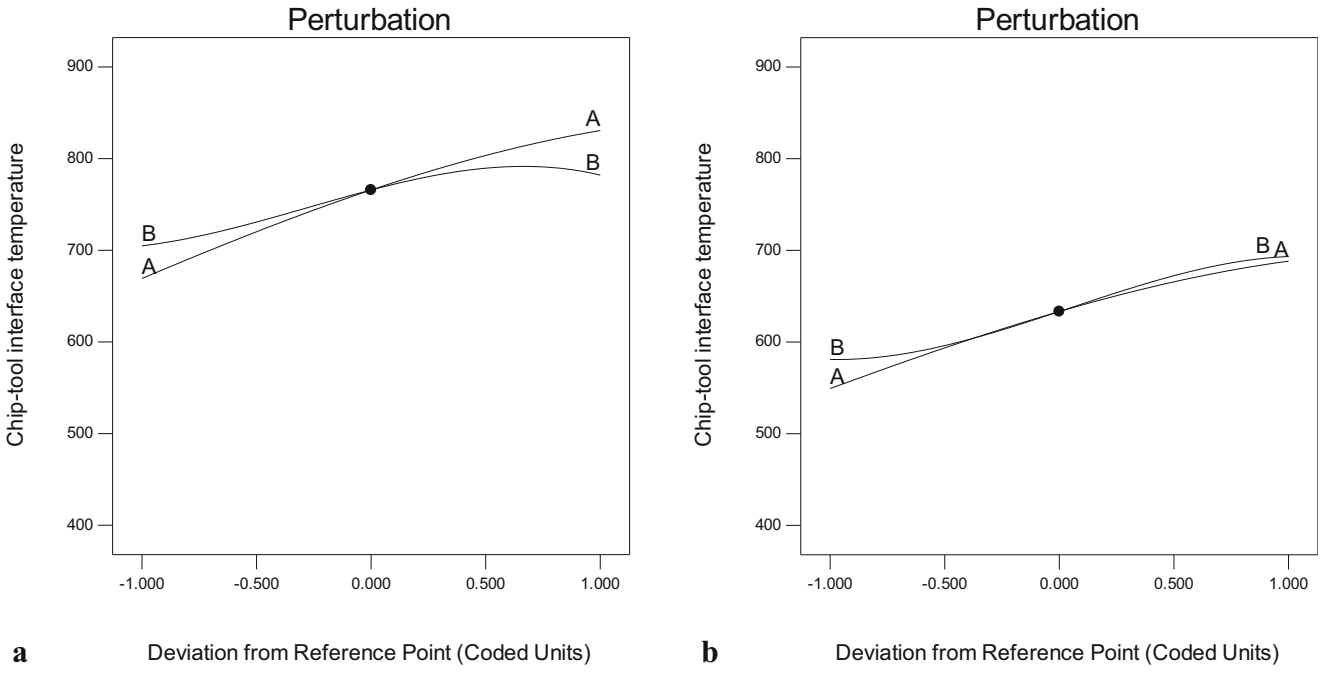

Fig. 3 Perturbation plot. **a** Dry, C-60 steel and SNMG insert. **b** HPC, 42CrMo4 steel, and SNMM

ANOVA (analysis of variance) for the response surface cubic model of chip–tool interface temperature is performed to check the quality of the model and determination of the effects of the selected process parameters on the measured response. Sum of squares (SS), degrees of freedom (DF), mean square (MS), F value, and Prob > F for all the factors along with their square, cubic, and interaction terms are shown in Table 6. SS is the sum of the squared deviations from the mean due to the effect of the corresponding terms. MS values stated in the third column of Table 6 are the variance associated with each particular term which is calculated by dividing SS by the DF. To

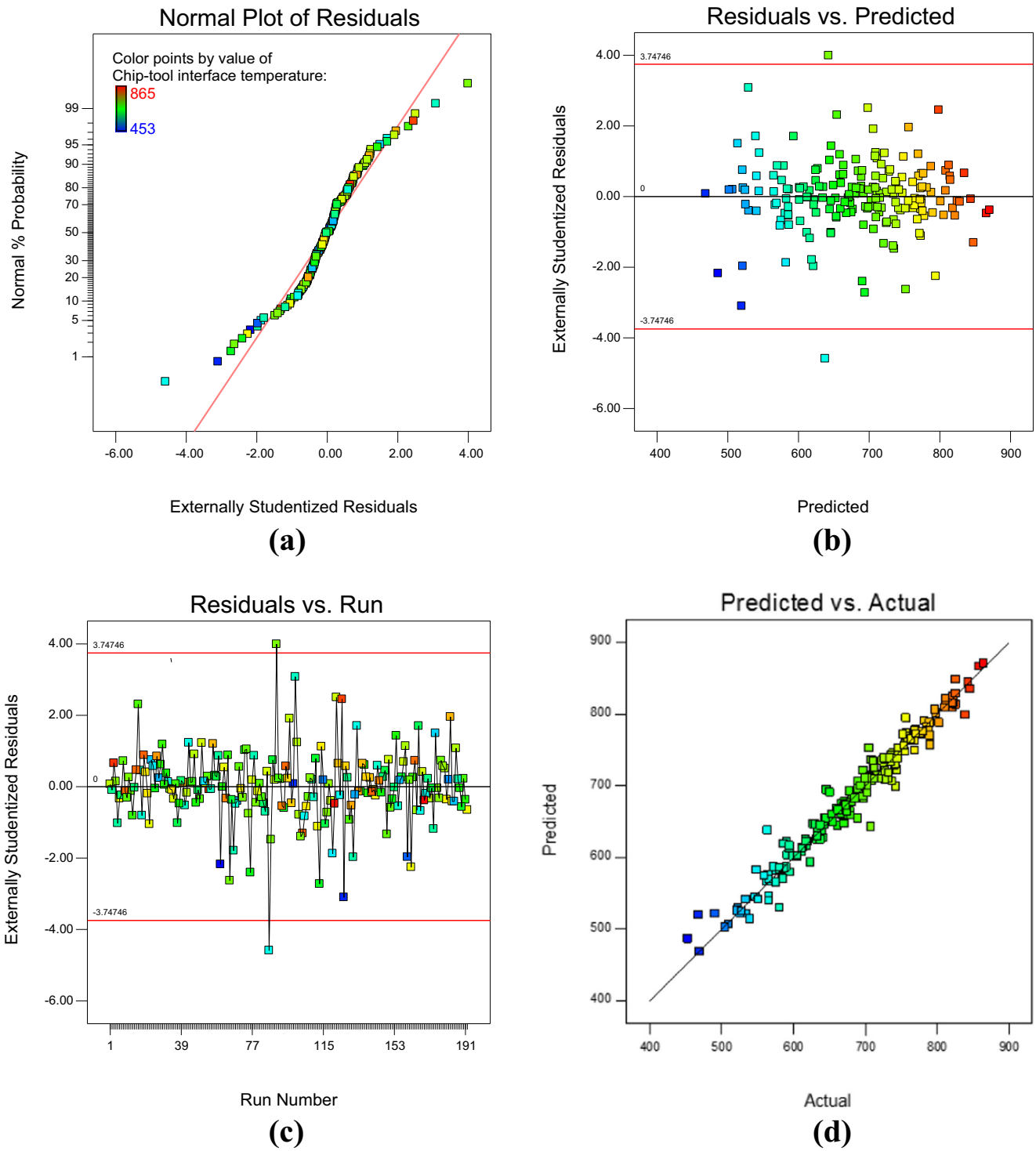

Fig. 4 Diagnostic graphs of the analysis. **a** Normal plot of residuals. **b** Residuals versus predicted. **c** Residuals versus run. **d** Predicted versus actual

compare the variance associated with a particular term with the residual variance, F value is calculated by dividing MS of that term by the MS for the residual. Prob > F is the probability of acquiring an F value of a particular size if the term did not have an effect on the response. Evaluating the results' statistical significance of a particular factor and the contribution it possesses in determining the response can be obtained. In general, a term that has a probability value less than 0.05 would be considered as statistically significant whereas a probability value greater than 0.10 is regarded as not significant.

In the chip–tool interface ANOVA, the model F value of 75.45 implies that the generated cubic model is statistically significant with Prob > F less than 0.0001. As stated earlier, any term is considered to be significant when value of Prob > F is less than 0.05; in this case, A, B, C, D, E, AC, AD, BC, BD, BE, CD, DE, A^2, BCD, BDE, B^2D, and B^3 are significant model terms. A-cutting speed has the highest F value and conveys the most remarkable influence on chip–tool interface temperature formation with ~38.82 % contribution which is in agreement with the studies published by Nayak M et al. [24], Gosai M et al. [25], Saglam H et al. [41], and Abhang L et al. [26]. Environment seems to be the second most dominant contributor with ~37.82 % contribution followed by feed with ~9.04 % contribution. Three different steels (Brinell hardness number (BHN) 195, 201, and 252) and two cutting inserts are also found to be significant model terms but with very little contribution of ~0.62 and ~0.14 %, respectively. The lower contribution level for residual (~3.6 %) justifies the validity of the model. The value of the adequate precision of the model which

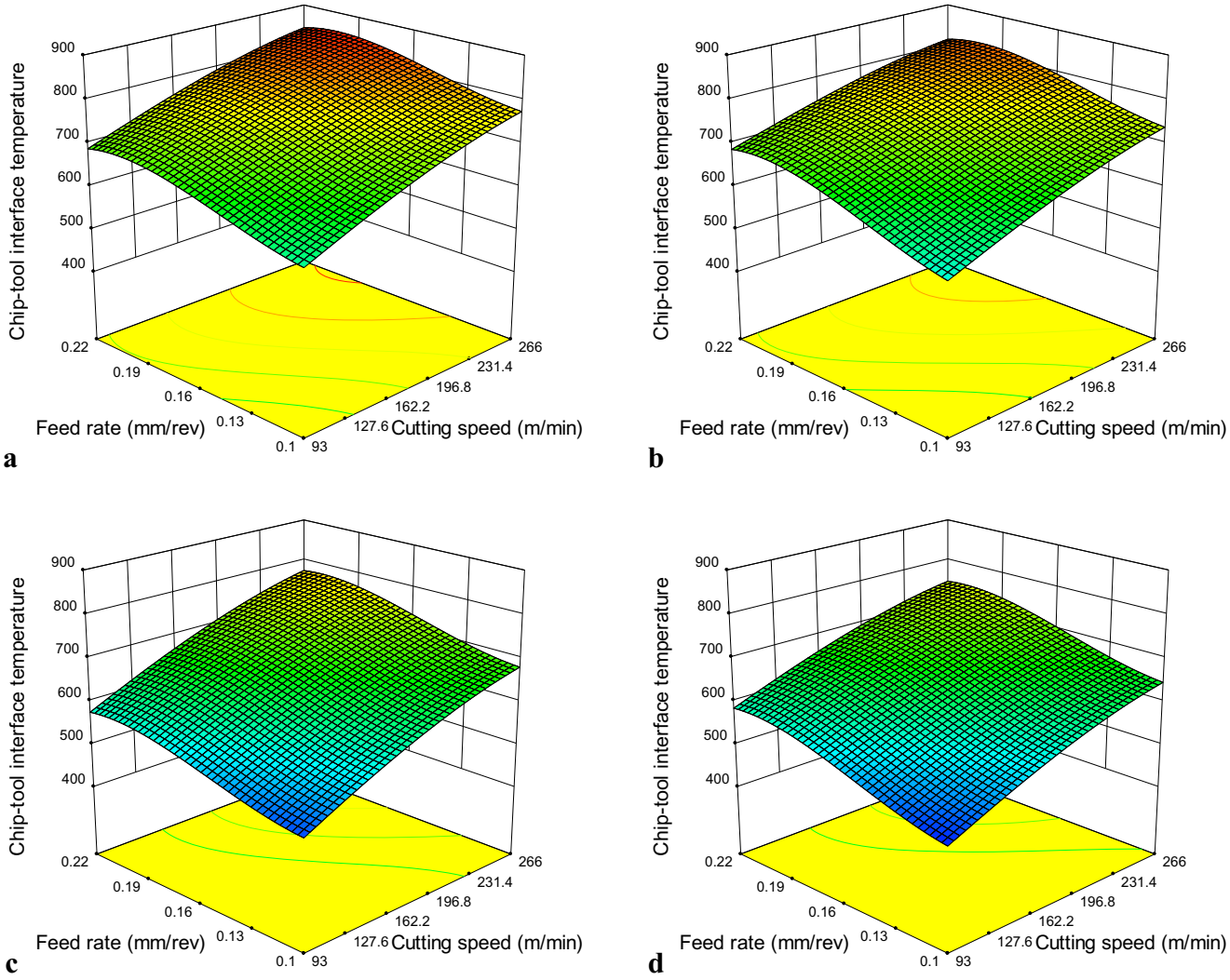

Fig. 5 The influence of cutting speed and feed rate on chip–tool interface temperature in turning C-60 steel under dry and HPC environment with SNMG and SNMM inserts. **a** Dry condition, SNMG insert. **b** Dry condition, SNMM insert. **c** HPC condition, SNMG insert. **d** HPC condition, SNMM insert

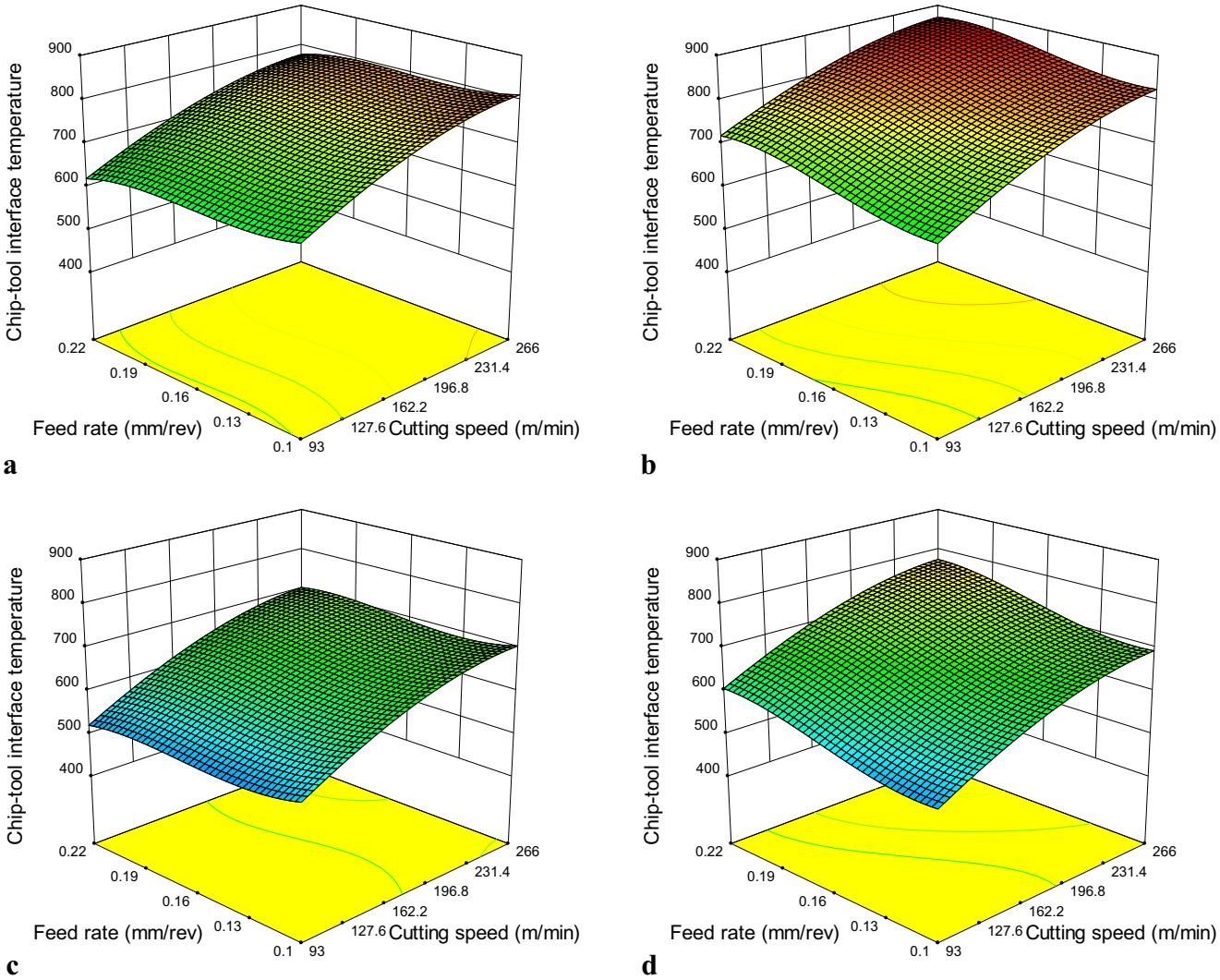

Fig. 6 The influence of cutting speed and feed rate on chip–tool interface temperature in turning 17CrNiMo6 steel under dry and HPC environment with SNMG and SNMM inserts. **a** Dry condition, SNMG insert. **b** Dry condition, SNMM insert. **c** HPC condition, SNMG insert. **d** HPC condition, SNMM insert

measures the signal to noise ratio is 39.770; usually, the ratio greater than 4 is desired to achieve a significant model for optimization. Standard deviation, mean value, and coefficient of variation (CV%) for the model are 19.61, 681.97, and 2.87, respectively. Furthermore, *R*-squared value for the model is 0.9640 which is much higher than the cutting temperature model developed by Nayak M et al. [24], where *R*-squared value of 0.8821 was obtained.

Response surface methodology is a collection of statistical and mathematical models that enable an experimental system in which a response of interest is influenced by several variables to make efficient empirical exploration of the system of interest [42, 43]. To exhibit the true functional relationship among the response and some independent variables, mathematical equation usually in the non-linear form can be developed to depict the system behavior more vividly. The response surface equations in terms of actual factors for each environment, material, and cutting insert obtained from ANOVA to make predictions about the response for given levels of each factors are shown in Eqs.1–12.

$$\Delta(C_1D_1E_1) = 688.143 + 1.482 \times \mathrm{A} - 6131.598 \times \mathrm{B} - 2.002 \times \mathrm{A} \times \mathrm{B} + 5.276\mathrm{E}{-}04 \times \mathrm{A}^2 + 52916.6 \times \mathrm{B}^2 + 1.07\mathrm{E}{-}03 \times \mathrm{A}^2 \times \mathrm{B} + 2.554 \times \mathrm{A} \times \mathrm{B}^2 - 5.233\mathrm{E}{-}06 \times \mathrm{A}^3 - 1.241\mathrm{E} + 05 \times \mathrm{B}^3 \quad (1)$$

$$\Delta(C_1D_1E_2) = 629.221 + 1.428 \times \mathrm{A} - 5645.405 \times \mathrm{B} - 2.912 \times \mathrm{A} \times \mathrm{B} + 7.975\mathrm{E}{-}04 \times \mathrm{A}^2 + 52330.663 \times \mathrm{B}^2 + 1.07\mathrm{E}{-}03 \times \mathrm{A}^2 \times \mathrm{B} + 2.555 \times \mathrm{A} \times \mathrm{B}^2 - 5.233\mathrm{E}{-}06 \times \mathrm{A}^3 - 1.241\mathrm{E} + 05 \times \mathrm{B}^3 \quad (2)$$

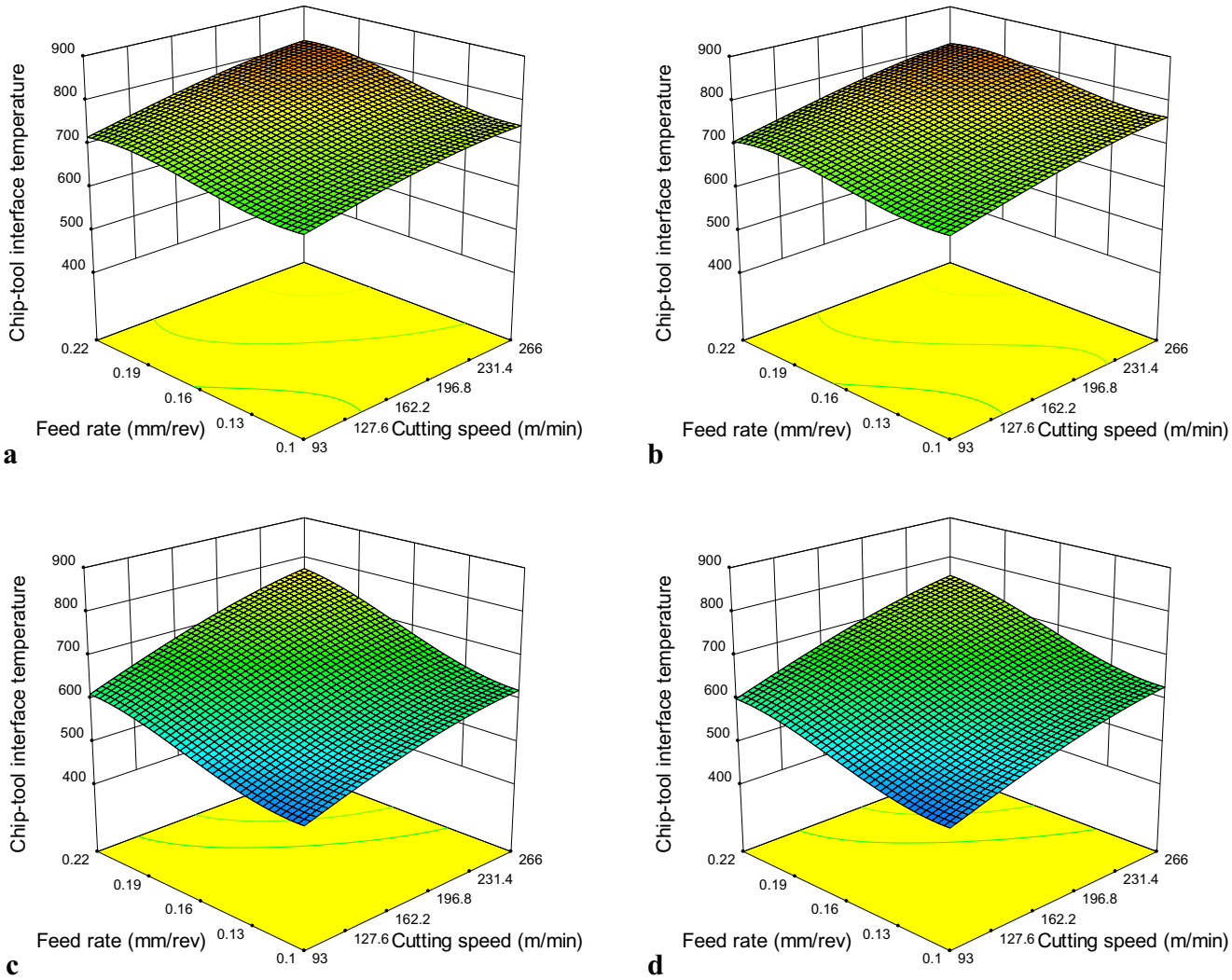

Fig. 7 The influence of cutting speed and feed rate on chip–tool interface temperature in turning 42CrMo4 steel under dry and HPC environment with SNMG and SNMM inserts. **a** Dry condition, SNMG insert. **b** Dry condition, SNMM insert. **c** HPC condition, SNMG insert. **d** HPC condition, SNMM insert

$$\Delta(C_1D_2E_1) = 932.954 + 2.009 \times A - 9029.236 \times B - 1.274 \times A \times B - 1.352E{-}03 \times A^2 + 58639.256 \times B^2 + 1.07E{-}03 \times A^2 \times B + 2.555 \times A \times B^2 - 5.233E{-}06 \times A^3 - 1.241E + 05 \times B^3 \quad (3)$$

$$\Delta(C_1D_2E_2) = 827.683 + 2.076 \times A - 7927.418 \times B - 2.183 \times A \times B - 1.082E{-}03 \times A^2 + 58053.319 \times B^2 + 1.07E{-}003 \times A^2 \times B + 2.555 \times A \times B^2 - 5.233E{-}06 \times A^3 - 1.241E + 05 \times B^3 \quad (4)$$

$$\Delta(C_1D_3E_1) = 996.995 + 0.52 \times A - 8381.892 \times B + 0.03 \times A \times B + 1.027E{-}03 \times A^2 + 58258.4 \times B^2 + 1.07E{-}03 \times A^2 \times B + 2.555 \times A \times B^2 - 5.233E{-}06 \times A^3 - 1.241E + 05 \times B^3 \quad (5)$$

$$\Delta(C_1D_3E_2) = 974.984 + 0.64 \times A - 8169.762 \times B - 0.88 \times A \times B + 1.296E{-}03 \times A^2 + 57672.459 \times B^2 + 1.07E{-}03 \times A^2 \times B + 2.555 \times A \times B^2 - 5.233E{-}06 \times A^3 - 1.241E + 05 \times B^3 \quad (6)$$

$$\Delta(C_2D_1E_1) = 604.615 + 1.743 \times A - 6990.623 \times B - 1.091 \times A \times B - 6.843E{-}05 \times A^2 + 55442.642 \times B^2 + 1.07E{-}03 \times A^2 \times B + 2.555 \times A \times B^2 - 5.233E{-}06 \times A^3 - 1.241E + 05 \times B^3 \quad (7)$$

$$\Delta(C_2D_1E_2) = 559.592 + 1.635 \times A - 6495.264 \times B - 2 \times A \times B + 2.014E{-}04 \times A^2 + 54856.704 \times B^2 + 1.07E{-}03 \times A^2 \times B + 2.555 \times A \times B^2 - 5.233E{-}06 \times A^3 - 1.241E + 05 \times B^3 \quad (8)$$

$$\Delta(C_2D_2E_1) = 850.41 + 2.179 \times A - 9797.636 \times B - 0.362 \times A \times B - 1.948E{-}03 \times A^2 + 61165.298 \times B^2 + 1.07E{-}03 \times A^2 \times B + 2.555 \times A \times B^2 - 5.233E{-}06 \times A^3 - 1.241E + 05 \times B^3 \quad (9)$$

$$\Delta(C_2D_2E_2) = 735.914 + 2.192 \times A - 8686.652 \times B - 1.272 \times A \times B - 1.678E{-}03 \times A^2 + 60579.361 \times B^2 + 1.07E{-}03 \times A^2 \times B + 2.555 \times A \times B^2 - 5.233E{-}06 \times A^3 - 1.241E + 05 \times B^3 \quad (10)$$

Table 7 Optimum values of factors and response for desirability optimization

Number	Cutting speed	Feed rate	Environment	Material	Cutting tool	Chip–tool interface temperature	Desirability	Decision
1	93.000	0.100	HPC	C-60	SNMM	468.776	0.962	Selected
2	93.000	0.101	HPC	C-60	SNMM	469.164	0.961	
3	95.561	0.100	HPC	C-60	SNMM	472.307	0.953	
4	93.000	0.112	HPC	C-60	SNMM	478.587	0.938	
5	93.000	0.100	HPC	C-60	SNMG	486.343	0.919	

$$\Delta(C_2D_3E_1) = 803.578 + 0.81 \times \mathrm{A} - 8756.23 \times \mathrm{B} + 0.942 \times \mathrm{A} \times \mathrm{B} + 4.306\mathrm{E}{-}04 \times \mathrm{A}^2 + 60784.439 \times \mathrm{B}^2 + 1.07\mathrm{E}{-}03 \times \mathrm{A}^2 \times \mathrm{B} + 2.555 \times \mathrm{A} \times \mathrm{B}^2 - 5.233\mathrm{E}{-}06 \times \mathrm{A}^3 - 1.241\mathrm{E} + 05 \times \mathrm{B}^3 \quad (11)$$

$$\Delta(C_2D_3E_2) = 782.531 + 0.965 \times \mathrm{A} - 8534.933 \times \mathrm{B} + 0.032 \times \mathrm{A} \times \mathrm{B} + 7.004\mathrm{E}{-}04 \times \mathrm{A}^2 + 60198.501 \times \mathrm{B}^2 + 1.07\mathrm{E}{-}03 \times \mathrm{A}^2 \times \mathrm{B} + 2.555 \times \mathrm{A} \times \mathrm{B}^2 - 5.233\mathrm{E}{-}06 \times \mathrm{A}^3 - 1.241\mathrm{E} + 05 \times \mathrm{B}^3 \quad (12)$$

Where C_n, D_n and E_n are representing categorical factors (referring to Table 2) while 'n' is representing level of the corresponding factor.

To compare the effects of all the factors at a particular point in the response surface design space, the perturbation graphs are plotted. The response is plotted by changing only one factor over its range while holding all the other factors constant. Example of two plots are shown in Fig. 3 at 179.5 m/min cutting speed and 0.16 mm/rev feed rate condition. Factor A: cutting speed has a steep slope or curvature which means the response is sensitive to this factor whereas a relatively flat line is observed for factor B: feed rate, this means that its change in the design space can be considered as insensitive. Similar conclusions were also drawn after evaluating ANOVA results, as cutting speed (~38.82 %) possessed relatively greater share of control on chip–tool interface temperature formation than feed rate (~9.04 %).

The normal probability plot shown in Fig. 4a indicates that the residuals follow a normal distribution as the points trail a straight line except some moderate scatter points. S-shaped curve visible in Fig. 4a is indicating that a transformation of the response may provide a better analysis. As calculated earlier, the ratio of the maximum to minimum value of the response is 1.90949, which suggested counteractive action of the suggestion given by the normal probability graph; although some trails were made by transforming (i.e., ArcSine square root, square root, natural log, power transformation, etc.) the response to observe the behavior of the system. As no significant effects were recorded, the initial design space is selected for further analysis. Figure 4b is the plot of the residuals versus ascending predicted response values. A random scatter within the range of ±3.74746 for externally studentized

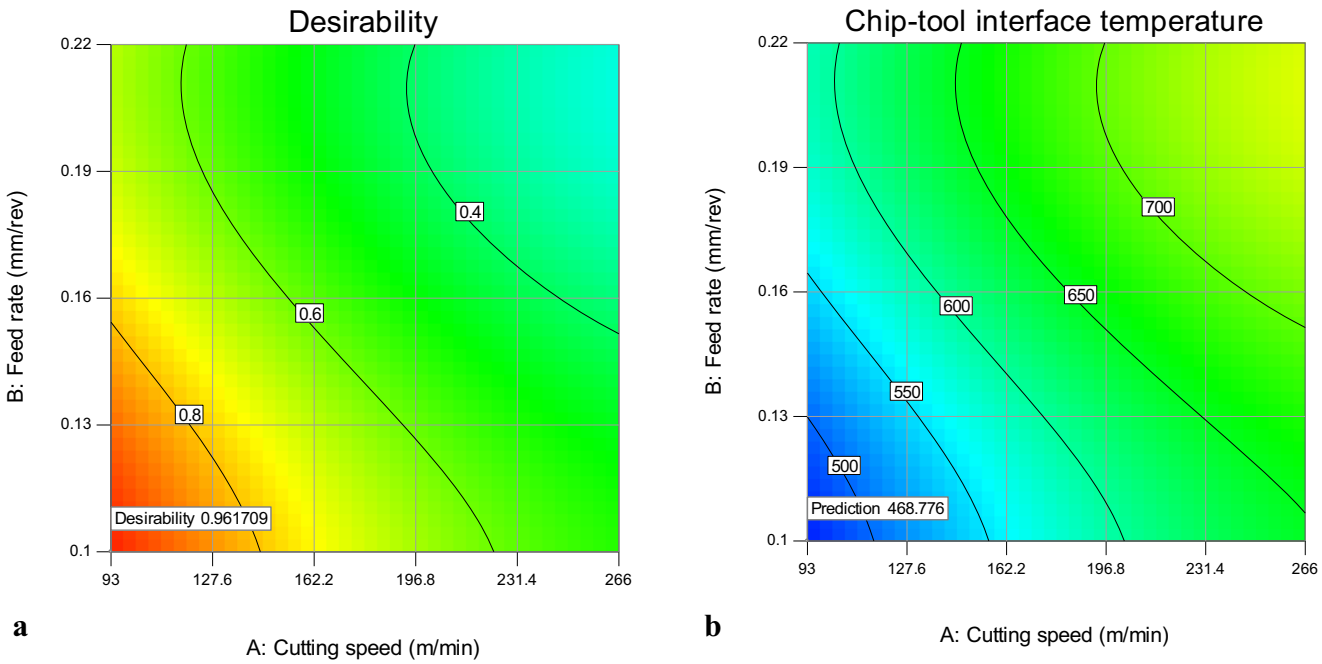

Fig. 8 Contour plot of desirability optimization. **a** Desirability. **b** Chip–tool interface temperature

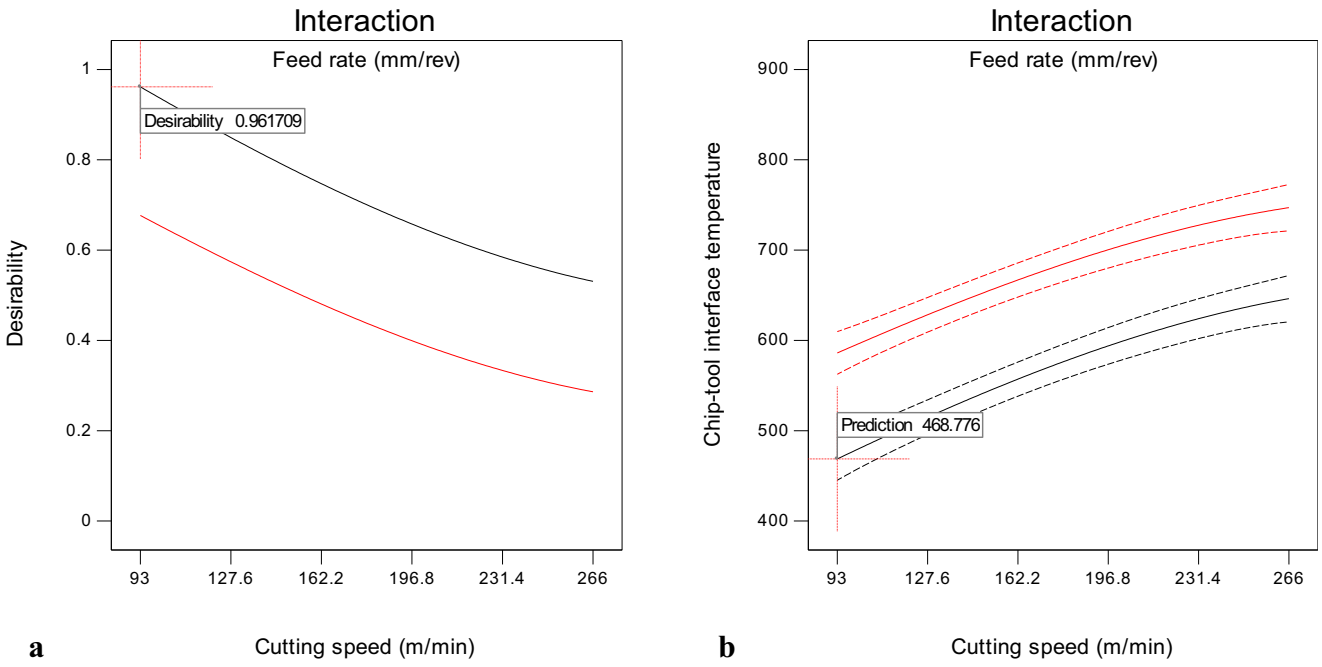

Fig. 9 Interaction plots of **a** desirability and **b** chip–tool interface temperature

residuals is observed in the figure along with two outliners which are runs with residuals outside the red lines on the plot. Run nos. 86 and 90 are the outliners which are not fitted well by the model. Two unusual observations are also visible in Fig. 4c where externally studentized residuals is plotted against the runs but all other points in the graph are randomly scattered. The observations which showed unusual trend were verified again and almost similar results were obtained after machining with proper set-up. The observed chip–tool interface temperatures against the predicted values are plotted in Fig. 4d. The data points are split evenly by the 45-degree line which demonstrates the adequacy of the model.

3.2 Analysis of high-pressure coolant effects

Analyzing the 3D surface plots (Figs. 5, 6, and 7) and Table 2, it has been observed that cooling effect is more at reduced cutting speed which agrees with the previous research works [2, 44]. Initially, the chip–tool contact is plastic but when the chip leaves the tool, the nature of contact is elastic; as a result, the high-velocity jet of high-pressure coolant is easily dragged in the elastic contact zone in a small quantity by capillary effect. It has also been observed that with an increase in cutting speed, the rate of chip–tool interface temperature reduction decreases, as with an increase in

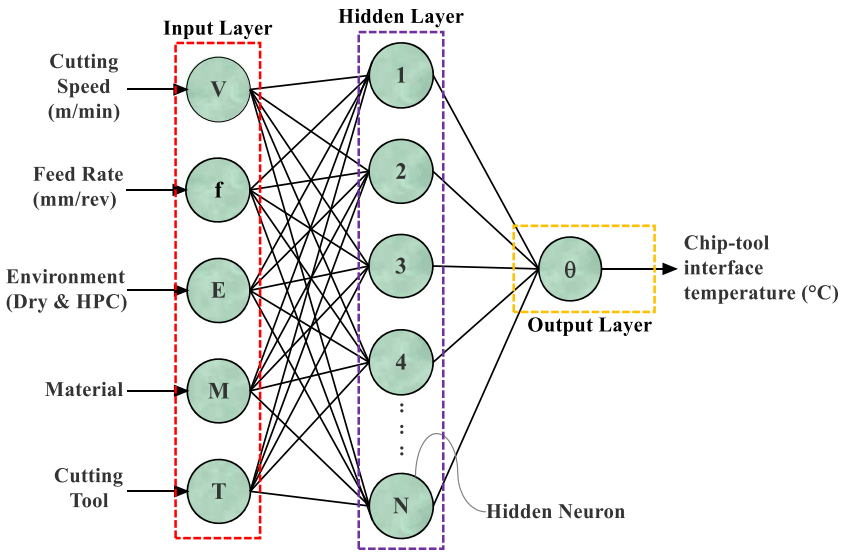

Fig. 10 Artificial neural network structure for average chip–tool interface temperature

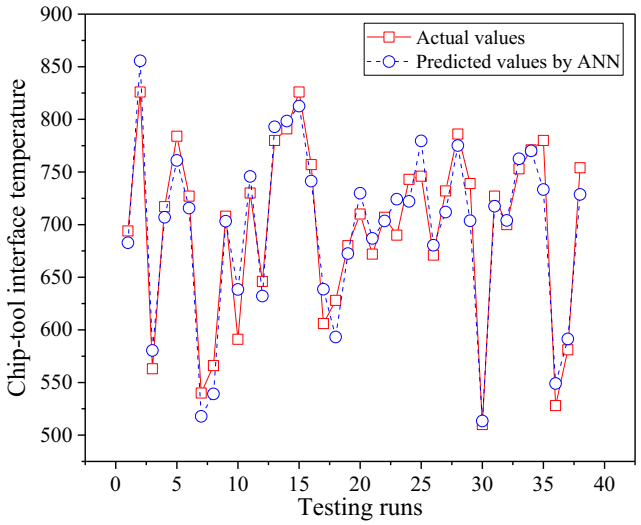

Fig. 11 Comparison between measured and predicted chip–tool interface temperature by ANN

cutting speed the chip makes fully plastic or bulk contact with the tool rake surface which prevents from entering of jet into the hot chip–tool interface. Again, at high velocity, little time is provided for the cutting fluid to penetrate, as a result, the coolant might not get enough time to remove the heat accumulated at the cutting zone resulting in less reduction in temperature under high-pressure cooling condition at a high level of cutting speeds [44]. Furthermore, the thinner chips are pushed up by the high-pressure coolant jet coming from the opposite direction of chip flow at lower chip velocity and enable it to come closer to the hot chip–tool contact zone to remove heat more effectively. Lifting up the chips with high-pressure coolant also facilitates chip breakability which indicates a decrease in shear angle. Curl radius of the thick chip is increased with an increase in feed rate; due to the effect, plastic contact length is increased and high-pressure coolant jet becomes less effective. For instance, in turning C-60 steel with SNMG insert at cutting speed = 93 m/min and feed rate = 0.1 mm/rev, the measured chip–tool interface temperature at dry condition is 592 °C while in HPC-assisted turning, it reduces to 453 °C and the percentage reduction rate is 23.48 %. At augmented cutting speed (266 m/min), the reduction rate reduces to 9.83 % for the same level of feed rate. Feed rate also largely affects the reduction rate. For example, at cutting speed of 186 m/min and 0.1 mm/rev feed rate, the rate of reduction is 16.67 % while it decreases to 16.15, 13.30, and 11.27 % for 0.14, 0.18, and 0.22 mm/rev feed rate, respectively. In turning 17CrNiMo4 steel with SNMG insert, at the lowest level of cutting speed and feed rate, the reduction rate of chip–tool interface temperature is 17.97 % which is much higher than 8.96 %, quantified at the highest level of cutting speed and feed rate. The range of reduction rate in turning 42CrMo4 steel with SNMG and SNMM inserts are 23.99–8.02 and 24.96–7.03 %, respectively. The SNMM insert having wide and deep slope parallel to its cutting edges seemed to provide better cooling effect than SNMG insert. Higher temperature was recorded in turning of 17CrNiMo4 and 42CrMo4 steel with SNMG insert and positively high reduction of chip–tool interface temperature is endorsed by SNMM insert.

Table 8 Performance evaluation of the models

	Type	RSM	ANN
MAPE (%)	Overall	1.750	0.858
	Testing	1.947	2.669
R-squared (R^2)	Overall	0.9640	0.9868
	Testing	0.9448	0.9325

3.3 Optimization by desirability function

Mono-objective numerical optimization by desirability function has been conducted to find factor settings that will satisfy the desired goals. The desired goal for each factor (in range) and response (minimize) is designated along with weight values. Same weights (=1) are assigned to each goal in this study to achieve uniform shape of its particular desirability function. Desirability described by Myers and Montgomery [42] is an objective function that ranges from 0 to 1. The numerical optimization finds a point that maximizes the desirability function as well as satisfies all the goals that have been addressed. To achieve a set of conditions that will satisfy all the goals is the main objective of the optimization, not to get to a desirability value of 1. Five optimum solutions are shown in Table 7 along with their desirability values. The set with the highest desirability has been selected. According to the best result (desirability = 0.962), the optimum cutting parameters which yield the lowest chip–tool interface temperature

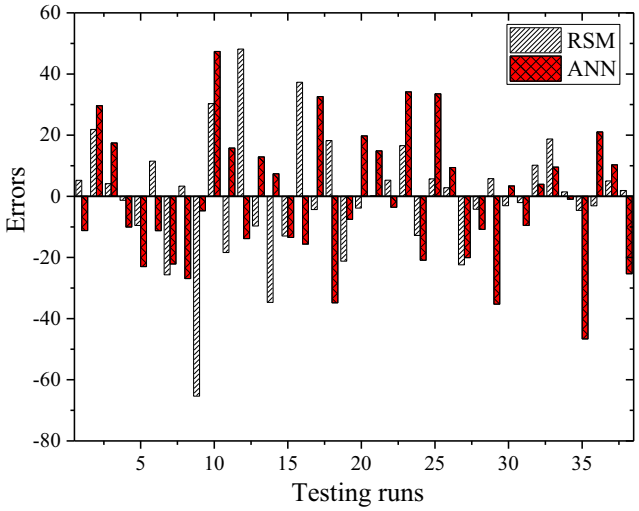

Fig. 12 Comparisons of prediction errors for testing runs

Table 9 Properties of the insert, work material, and cutting oil

Insert	C-60		Cutting oil			
Thermal conductivity (λ_t)	Thermal conductivity (λ)	Thermal diffusivity (a_c)	Density (ρ)	Prandtl number (Pr)	Absolute viscosity (υ)	Thermal conductivity (λ_0)
0.47 J/cm s °C	0.43 J/cm s °C	3.84 cm^2/s	882×10^{-6} Kg/cm^3	754	68×10^{-6} m^2/s	0.0015 J/cm s °C

(~468.776 °C) are as follows: cutting speed = 93 m/min, feed rate = 0.10 mm/rev, material = C-60 steel, cutting tool = SNMM, and most eminently, machining environment = HPC. The lowest level of cutting speed (78 m/min) and feed rate (0.12 mm/rev) in HPC-assisted turning is necessary for minimum cutting temperature is suggested in the research work by Mia et al. [45], where the Taguchi and Gray-Taguchi methods were used to optimize machining parameters during turning of Ti-6Al-4V alloy. As the optimum-factor setting was already on the current design space, so a performance measure of the desirability function is done by comparing the specific given temperature in solution 1 with the actual value. Absolute percentage error (APE) of 3.48 % is calculated for this particular solution. For further inspection, contour plot of desirability optimization is illustrated in Fig. 8. While Fig. 9 depicts the interaction plots of desirability and predicted chip–tool interface temperature. According to Fig. 9a, desirability value is maximum (0.961709) at the lowest level of cutting speed and with the progression of cutting speed, desirability value decreases. The slope of the curves (B − 0.1 and B + 0.22) form a similar pattern although lower desirability value is obtained at the curve of feed rate = 0.22 mm/rev. Figure 9b conveys the message that augmented cutting speed and feed rate are affiliated with elevated chip–tool interface temperature.

3.4 Prediction by ANN

Artificial neural network is an AI-based simulation tool competent of non-linear modeling of inputs and outputs more efficiently compared to conventional techniques in terms of accuracy, speed, and simplicity. ANN is capable to learn and implement as like functionality of the human brain learning process as well as to adapt changes altering various weighted connections and biases which interconnects nodes called neurons contained in different layers of ANN architecture. Generally, three layers construct the anatomy of an ANN model: (a) input layer, (b) hidden layer, and (c) output layer. Input layer comprises of some control variables represented by neurons that have authority over the output of the neural network. The output layer of the neural network is what actually presents the numerical values of the responses or variables that are dependent. The intermediate layer also known as the hidden layer consists of hidden neurons which play a noteworthy role in the overall performance of the neural network specially in case of dealing with complex, noisy, and comparatively large problems. Process of determining the optimum number of hidden neurons is much confusing and not yet stated properly though many researches have been performed on this specific topic throughout the last decade. If the number of hidden neurons are less compared to the complexity of the input–output relationship, then under fitting may occur whereas if excess number of neurons populates the hidden layer than performance of the neural network will deteriorate mainly because of overfitting. Modeling of ANN consists of two distinct phases: training and testing. During the training phase, numerical values of the predictor factors or numerical representation of any categorical factor acting as a predictor are given to the input neurons located at the input layer and their corresponding responses are given to the output neurons, in the form of matrices on any compatible computational environment (Matlab, Java, etc.). After training, unseen data of the predictors can be provided to the input neurons to get the predicted values of the responses through the output neurons.

In this article, feedforward back propagation neural network [46] is developed with five input neurons and one output neuron which provides the predicted values of chip–tool interface temperature. The numerical values of cutting speeds (v); feed rates (f); and categorical values of machining environments (dry and HPC); materials (C-60, 17CrNiMo6, and 42CrMo4 steel); and cutting inserts (SNMG and SNMM) are given to the network as

Table 10 Tool life of SNMG and SNMM insert at VB = 300 μm

Cutting speed (m/min)	Feed rate (mm/rev)	SNMG insert			SNMM insert		
		Tool life (min)			Tool life (min)		
		Dry	HPC	% increment	Dry	HPC	% increment
133	0.14	59	91	54	35	84	140
	0.18	45	73	62	29	67	131
	0.22	41	67	63	23	50	117
152	0.14	44	71	61	30	62	107
	0.18	35	53	51	24	50	108
	0.22	30	42	40	17	31	82
186	0.14	40	53	33	25	50	100
	0.18	24	42	75	19	40	111
	0.22	21	36	71	12	22	83

Table 11 Analysis of variance for tool life

Source	DF	Sum of squares	Mean square	*F* value	*P* value Prob > *F*
Cutting speed	2	3335	1667.36	47.65	0.000
Feed rate	2	2662	1331.03	38.04	0.000
Environment	1	5160	5160.03	147.46	0.000
Cutting tool	1	1078	1078.03	30.81	0.000
Error	29	1015	34.99		
Total	35	13,250			

input. A total of 192 data sets are divided into two parts: 154 data sets are used to train the ANN model and 38 data sets are separated in order to test the accuracy of the developed model. Normalization of the data set is not adopted in the present study. It is important to keep in mind that testing data does not have any effect during training. The training of the networks is done on MATLAB R2015a, neural network toolbox 7 [47]. Figure 10 represents a model structure of the neural network considered in this study. Single hidden layer is adopted to construct the networks but the number of hidden neurons varied. In this article, 22 hidden neurons have been chosen after evaluating the results found during testing the networks in terms of MAPE, configured with 3 to 25 hidden neurons.

The networks are trained using Bayesian regularization (BR) algorithm as it is proven to perform well as stated by Mia and Dhar [48]. Artificial neural networks trained operating with Bayesian regularization generates the potential to reduce or ignore the lengthy cross-validation process and has the ability to handle imprecise noisy data [49–51]. Two transfer functions have been used to devolve the models: hyperbolic tangent sigmoid transfer function (hidden layer) and linear transfer function (output layer). The performance function adopted for the networks are mean square error (MSE). After the training phase, simulations have been made using unseen data to test the prediction capability of the developed model. Following the training-testing procedure for selecting number of neurons in hidden layer employed by T. Özel [30], five trials of training and testing phase are performed for each network structure for precise evaluation. Training multiple times generated different results within close proximity for same structures because of the different initialization values of weights and biases.

$$\mathrm{MSE} = \frac{1}{N}\sum_{n=1}^{N}(\mathrm{Actual}-\mathrm{Predicted})^2 \tag{13}$$

$$\mathrm{MAPE} = \frac{1}{N}\sum_{n=1}^{N}\left(\frac{|\mathrm{Actual}-\mathrm{Predicted}|}{\mathrm{Actual}}\right)\times 100 \tag{14}$$

The prediction accuracy of the networks are measured using mean absolute percentage error (MAPE). The lowest MAPE during testing phase is found to be 2.669 % for 4-22-1 neural network configuration trained with BR algorithm. Figure 11 illustrates the prediction accuracy of the developed ANN prediction model (4-22-1). Predicted values and actual measured values of chip–tool interface temperature of 38 data sets chosen for the testing purpose is plotted against the testing runs to ascertain the amount of aberration. On assessing the graphs, it could be summarized that the network structure has given quite a similar line pattern for actual and predicted values. Linear regression is calculated for these selected data set to measure the prediction capability. Linear regression *R* value is found to be 0.9660, the high value of regression reflects the high accuracy and acceptability of the formulated model.

3.5 Comparison of the prediction models

In this section, a comparison is supervised between the two prediction techniques analyzed in erstwhile sections to predict chip–tool interface temperature. The all-inclusive performance (training and testing) and testing accuracy of these techniques are evaluated in terms of MAPE and coefficient of determination (R^2); the results are explicitly shown in Table 8. As stated earlier, 38 data sets were used to test the adequacy of the ANN model and MAPE quantified at the testing phase is 2.669 %. To present a comparison with RSM model, Eqs. 1–12 are used to predict the response for the same testing data set which was used in case of ANN.

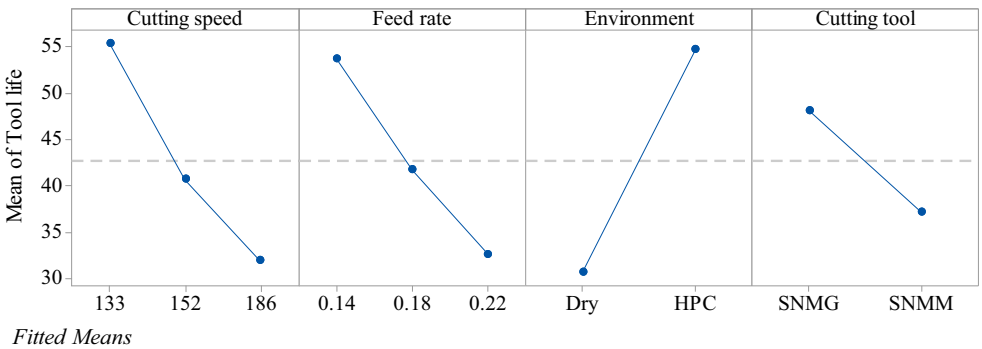

Fig. 13 Mean effect plot of tool life

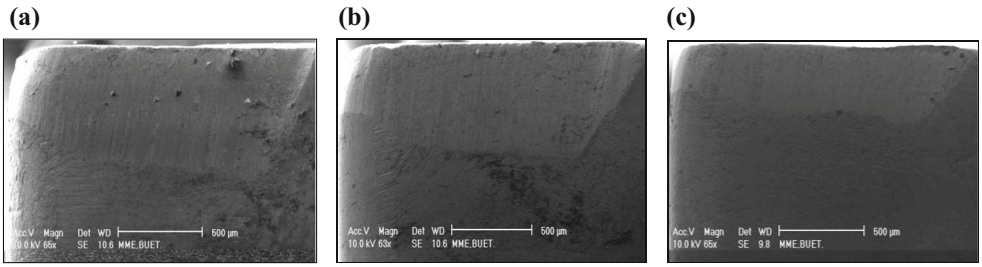

Fig. 14 SEM views of principal flank of worn out tip of SNMG insert after machining C-60 steel under **a** dry condition, 48 min; **b** wet condition, 48 min; and **c** HPC condition, 48 min

MAPE of 1.947 % is accounted for the RSM model, which is slightly more accurate than the neural network model. Again, MAPE is calculated for predictions of all 192 data sets including both training and testing domain which reveals that ANN model performed better with 0.892 % improvement in accuracy. In terms of R^2 value, overall ANN model outperformed the performance of the overall RSM model, similar outcome was also reported in research works published by Karkalos N et al. [20] and Mia and Dhar [52]. However, higher coefficient of determination was observed in case of developed equations for RSM within testing domain which is in accordance with the analysis made by R. Kumar et al. [32]. Furthermore, Ihsan Korkut et al. [37] showed ANN can perform better than regression models when chip–tool interface temperature prediction ability was measured. Figure 12 illustrates the graphical comparison of errors found during testing phase of the models.

3.6 Tool life

Tool life can be defined as the length of cutting time that the tool can be used until final catastrophic failure. The main three reasons behind the failure of a cutting tool in machining are (i) fracture failure, (ii) temperature failure, and (iii) gradual wear [53]. The fracture failure occurs when the cutting force at the tool point becomes excessive, causing it to fail suddenly by brittle fracture. When the cutting temperature is too high for the tool material, temperature failure occurs which leads to plastic deformation of the tool and loss of the sharp edge. These two types of failures result in premature loss of the cutting tool. Again, cutting tools in conventional machining, particularly in continuous chip formation processes like turning, generally fails by gradual wear (i.e., abrasion, adhesion, diffusion, chemical erosion, galvanic action) depending upon the tool–work materials and machining condition. In the present investigation with the tools and work material and the machining conditions undertaken, the tool failure mode has been mostly gradual wear, more specifically, adhesion or attrition wear [54]. The material properties of the uncoated carbide tool inserts (SNMG 120408 and SNMM 120408), the workpiece, and the coolant are listed in Table 9.

The effect of application of jet impingement at elevated pressure over traditional dry-cut machining on tool life of SNMG and SNMM inserts at different *v*–*f* combination in turning C-60 steel can be divulged from the summary of the times to failure for all test conditions stated in Table 10. The cutting speeds chosen for the experiment are 133, 152, and 186 m/min while feed rate is kept within the range of 0.14 and 0.22 mm/rev and depth of cut is held constant at 1.5 mm. Significant improvement of tool life under the application of high-pressure coolant jet is perceptible from Table 10, where in case of uncoated carbide SNMM insert, up to 140 % increment over dry-cut is achieved. Time, until the rejection of a tool, decreases at augmented cutting speed and feed rate due to higher friction and heat generation [18]. For example, at cutting speed of 133 m/min and feed rate of 0.14 mm/rev, the life of the SNMG insert is 59 min for dry-cut and 91 min for HPC-assisted machining. Tool life decreases to 21 min during machining under the absence of cutting fluids and 36 min for machining with high-pressure coolant at higher level of cutting speed, 186 m/min and feed rate, 0.22 mm/rev. Identical relation is also observable by analyzing the measured tool life for SNMM insert. Moreover, high-pressure coolant drastically ameliorates tool condition by the reduction of adhered material on flank and rake face [19]. Again, reduction of auxiliary flank wear due to retention of tool hardness promoted by reduction of chip–tool interface temperature in HPC-assisted cutting, aid to achieve prolong tool life [55]. It is also evident

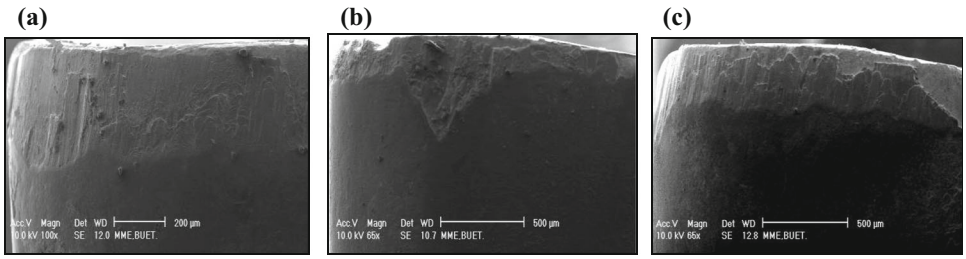

Fig. 15 SEM views of principal flank of worn out tip of SNMM insert after machining C-60 steel under **a** dry condition, 48 min; **b** wet condition, 48 min; and **c** HPC condition, 48 min

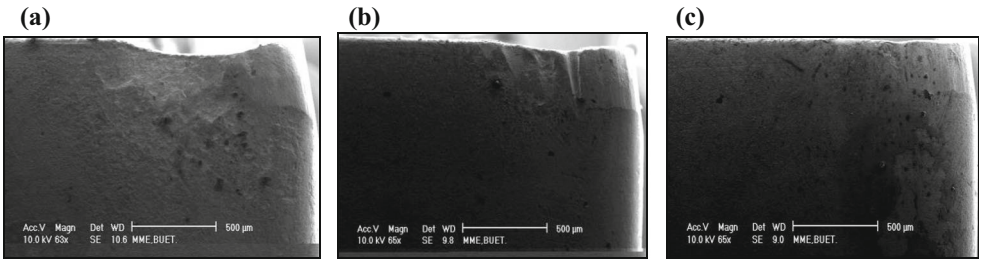

Fig. 16 SEM views of auxiliary flank of worn out tip of SNMG insert after machining C-60 steel under **a** dry condition, 48 min; **b** wet condition, 48 min; and **c** HPC condition, 48 min

from Table 10 that percentage increment rate of SNMM tool life dwindles with the progression of cutting speed. However, no such pattern can be depicted for SNMG insert.

ANOVA for tool life is presented in Table 11. All four process factors associated with the analysis are significant model terms as P value is less than 0.05. The influence of machining environment, dry, and HPC-assisted, is found to be the most dominant factor with ~38.94 % contribution on the formation of tool life model. Cutting speed has the second most commanding effect with ~25.17 %, followed by feed rate with ~20.1 %, and tool characteristics with ~8.1 % contribution. The contribution of the error term is ~7.7 %. R-squared value of the model is found to be 92.34 %, whereas adjusted R-squared and predicted R-squared are 90.76 and 88.20 %. Two unusual observations are found which are run nos. 19 and 28. The mean effect plot is framed in Fig. 13.

The SEM views, for micro-scale observation, of SNMG and SNMM inserts after 48 min of continuous machining of C-60 steel at 193 m/min cutting speed and 0.18 mm/rev feed and 1.5-mm depth of cut in dry-cut, conventional wet, and HPC-assisted cooling mechanism are framed in Figs. 14, 15, 16, and 17. It is discernable from the micro-level representation that conventional soluble oil cutting fluid did not significantly ameliorate the nature and extent of wear as such turning steels with the usage of conventional wet cooling causes faster oxidation and corrosion of the tool surfaces and rapid micro fracturing of the cutting edges by thermo-mechanical shocks. Whereas application of elevated pressure has provided remarkable improvement [56] and even after 48 min of machining, both flank and crater wear have been much uniform and much smaller in magnitude and only a small notch appeared on the auxiliary flank. Such improvement by HPC jet can be attributed mainly to retention of hardness and sharpness of the cutting edge for their steady and intensive cooling, protection from oxidation and corrosion and absence of built-up edge (BUE) formation, which accelerates both crater and flank wear by flaking and chipping.

4 Conclusions

In this research paper, turning at different cutting speed and feed rate combinations of commonly used C-60, 17CrNiMo4, and 42CrMo4 steel alloys in dry and HPC-assisted machining with SNMG and SNMM cutting inserts have been conducted to evaluate the performance of application of jet stream at elevated pressure on chip–tool interface temperature as well as tool life. Furthermore, development of predictive models of cutting temperature with the help of RSM and ANN along with performance measure of the aforementioned models, is another concern of the analysis. The following conclusions can be drawn based on the results of the present investigation:

1. A total of 192 observations have been conducted based on full factorial design plan and RSM has been employed for subsequent modeling to formulate mathematical equations to make accurate predictions of chip–tool interface temperature. ANOVA has been performed to evaluate the effects of cutting speed, feed rate, environment, material, and cutting insert as well as their interactions terms on the formation of chip–tool interface temperature and to measure the significance of the proposed model. R^2 value for the model is 0.9640 and the model F value of 75.45 implies that the model is statistically significant.
2. Cutting speed has relatively greater share of control on chip–tool interface temperature formation with

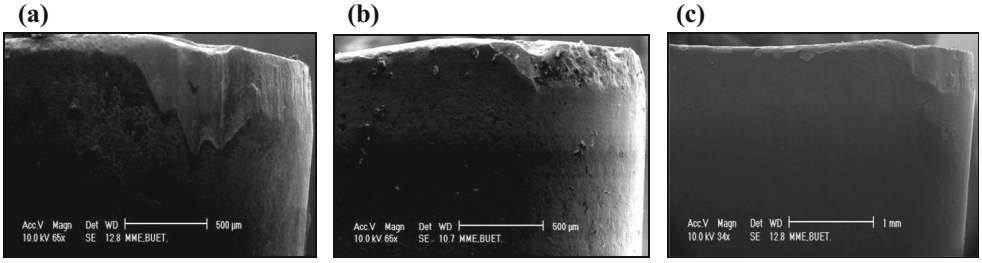

Fig. 17 SEM views of auxiliary worn out tip of SNMM insert after machining C-60 steel under **a** dry condition, 48 min; **b** wet condition, 48 min; and **c** HPC condition, 48 min

~38.82 % contribution. Environment has the second most influential effect in this analysis accounting for ~37.82 % contribution followed by feed rate with ~9.04 % contribution. Materials and cutting inserts possessed very little effects where ~0.62 and ~0.14 % contribution are accounted respectively.

3. The lowest measurement of chip–tool interface temperature is achieved at the lowest level of cutting speed and feed rate in turning of C-60 steel (BHN: 195) with SNMM cutting insert in HPC-assisted machining. Optimization with desirability function manifested exact set of factors and absolute percentage error (APE) between the predicted response and actual experimental value on the aforesaid conditions is 3.48 %. Noteworthy, the calculated value of desirability is 0.960.
4. Feedforward back propagation neural networks trained using Bayesian regularization algorithm have been developed with five input neurons and one output neuron to predict the values of chip–tool interface temperature. The lowest MAPE during testing phase is found to be 2.669 % for 4-22-1 neural network configuration and overall MAPE including both training and testing phase is 0.858 %. R^2 value for the overall performance phase and testing phase are 98.68 and 93.25 %, respectively.
5. The mathematical equations formulated using RSM have evinced less MAPE compared to ANN model during testing phase. MAPE quantified for total 192 observations and the testing data set are 1.750 and 1.947 %, respectively. Again, predicted R^2 value for the overall performance is 96.40 % whereas testing data reckoned at 94.48 %.
6. HPC-assisted machining promotes improved tool life where up to 140 % improvement over dry machining is observable. Even after 48 min of machining, it has been scrutinized from SEM figures that HPC jet has provided remarkable improvement of tool condition on both principal and auxiliary flank whereas conventional soluble cutting fluid did not significantly improve the nature and extent of wear. Environment (dry and HPC) is the most dominant factor which has ~38.94 % contribution on tool life followed by cutting speed with ~25.17 % contribution, according to ANOVA for tool life.

References

1. Dhar N, Kamruzzaman M (2007) Cutting temperature, tool wear, surface roughness and dimensional deviation in turning AISI-4037 steel under cryogenic condition. Int J Mach Tools Manuf 47(5): 754–759
2. Kamruzzaman M, Dhar N (2008) The effect of applying high-pressure coolant (HPC) jet in machining of 42CrMo4 steel by uncoated carbide inserts. J Mech Eng 39(2):71–77
3. Çakıroğlu R, Acır A (2013) Optimization of cutting parameters on drill bit temperature in drilling by Taguchi method. Measurement 46(9):3525–3531
4. Sun S, Brandt M, Palanisamy S, Dargusch MS (2015) Effect of cryogenic compressed air on the evolution of cutting force and tool wear during machining of Ti–6Al–4V alloy. J Mater Process Technol 221:243–254
5. Sales WF, Diniz AE, Machado ÁR (2001) Application of cutting fluids in machining processes. J Braz Soc Mech Sci 23(2):227–240
6. Wertheim R, Rotberg J, Ber A (1992) Influence of high-pressure flushing through the rake face of the cutting tool. CIRP Ann-Manuf Technol 41(1):101–106
7. Raynor PC, Cooper S, Leith D (1996) Evaporation of polydisperse multicomponent oil droplets. Am Ind Hyg Assoc J 57(12):1128–1136
8. Umbrello D, Micari F, Jawahir I (2012) The effects of cryogenic cooling on surface integrity in hard machining: a comparison with dry machining. CIRP Ann-Manuf Technol 61(1):103–106
9. Islam AK, Mia M, Dhar NR (2016) Effects of internal cooling by cryogenic on the machinability of hardened steel. Int J Adv Manuf Technol:1–10. doi:10.1007/s00170-016-9373-y
10. Dhar N, Islam M, Islam S, Mithu M (2006) The influence of minimum quantity of lubrication (MQL) on cutting temperature, chip and dimensional accuracy in turning AISI-1040 steel. J Mater Process Technol 171(1):93–99
11. Amini S, Paktinat H (2014) Ceramic tools with ordinary and wiper inserts in near dry machining with high speed on super alloy Monel K500. Mater Manuf Process 29(5):579–584
12. Mia M, Dhar NR (2016) Optimization of surface roughness and cutting temperature in high-pressure coolant-assisted hard turning using Taguchi method. Int J Adv Manuf Technol:1–15. doi:10.1007/s00170-016-8810-2
13. Sharman A, Hughes J, Ridgway K (2008) Surface integrity and tool life when turning Inconel 718 using ultra-high pressure and flood coolant systems. Proc Inst Mech Eng B J Eng Manuf 222(6):653–664
14. Bermingham M, Palanisamy S, Kent D, Dargusch M (2012) A comparison of cryogenic and high pressure emulsion cooling technologies on tool life and chip morphology in Ti–6Al–4V cutting. J Mater Process Technol 212(4):752–765
15. Ezugwu E (2005) Key improvements in the machining of difficult-to-cut aerospace superalloys. Int J Mach Tools Manuf 45(12):1353–1367
16. Wright P, Horne J, Tabor D (1979) Boundary conditions at the chip-tool interface in machining: comparisons between seizure and sliding friction. Wear 54(2):371–390
17. Ezugwu E, Da Silva R, Bonney J, Machado A (2005) Evaluation of the performance of CBN tools when turning Ti–6Al–4V alloy with high pressure coolant supplies. Int J Mach Tools Manuf 45(9): 1009–1014
18. Braham-Bouchnak T, Germain G, Morel A, Furet B (2015) Influence of high-pressure coolant assistance on the machinability of the titanium alloy Ti555-3. Mach Sci Technol 19(1):134–151
19. Naves V, Da Silva M, Da Silva F (2013) Evaluation of the effect of application of cutting fluid at high pressure on tool wear during turning operation of AISI 316 austenitic stainless steel. Wear 302(1):1201–1208
20. Karkalos N, Galanis N, Markopoulos A (2016) Surface roughness prediction for the milling of Ti–6Al–4V ELI alloy with the use of statistical and soft computing techniques. Measurement 90:25–35
21. Bouzid L, Yallese MA, Chaoui K, Mabrouki T, Boulanouar L (2015) Mathematical modeling for turning on AISI 420 stainless steel using surface response methodology. Proc Inst Mech Eng B J Eng Manuf 229(1):45–61
22. Rajmohan T, Sathishkumar S, Palanikumar K, Ranganathan S (2015) Modeling and analysis of cutting force in turning of AISI 316L Stainless Steel (SS) under nano cutting environment. Appl Mech Mater

23. Berkani S, Bouzid L, Bensouilah H, Yallese MA, Girardin F, Mabrouki T (2015) Modeling and optimization of tool wear and surface roughness in turning of austenitic stainless steel using response surface methodology. S09d Procédés d'usinage
24. Nayak M, Sehgal R (2015) Effect of tool material properties and cutting conditions on machinability of AISI D6 steel during hard turning. Arab J Sci Eng 40(4):1151–1164
25. Gosai M, Bhavsar SN (2016) Experimental study on temperature measurement in turning operation of hardened steel (EN36. Procedia Technol 23:311–318
26. Abhang L, Hameedullah M (2010) Chip-tool interface temperature prediction model for turning process. Int J Eng Sci Technol 2(4): 382–393
27. Sharma MD, Sehgal R (2015) Modelling of machining process while turning tool steel with CBN tool. Arab J Sci Eng:1–22
28. Çalışkan H, Kurbanoğlu C, Panjan P, Kramar D (2013) Investigation of the performance of carbide cutting tools with hard coatings in hard milling based on the response surface methodology. Int J Adv Manuf Technol 66(5–8):883–893
29. Amini S, Fatemi M, Atefi R (2014) High speed turning of Inconel 718 using ceramic and carbide cutting tools. Arab J Sci Eng 39(3): 2323–2330
30. Özel T, Karpat Y (2005) Predictive modeling of surface roughness and tool wear in hard turning using regression and neural networks. Int J Mach Tools Manuf 45(4):467–479
31. Rao KV, Murthy B, Rao NM (2014) Prediction of cutting tool wear, surface roughness and vibration of work piece in boring of AISI 316 steel with artificial neural network. Measurement 51:63–70
32. Kumar R, Chauhan S (2015) Study on surface roughness measurement for turning of Al 7075/10/SiCp and Al 7075 hybrid composites by using response surface methodology (RSM) and artificial neural networking (ANN. Measurement 65:166–180
33. Jayakumar K, Mathew J, Joseph M (2013) An investigation of cutting force and tool–work interface temperature in milling of Al–SiCp metal matrix composite. Proc Inst Mech Eng B J Eng Manuf 227(3):362–374
34. Adesta EYT, Al Hazza MH, Suprianto M, Riza M (2012) Prediction of cutting temperatures by using back propagation neural network modeling when cutting hardened H-13 steel in CNC end milling. In: Advanced Materials Research. Trans Tech Publ:91–94
35. Tanikic D, Manic M, Devedzic G, Cojbasic Z (2010) Modelling of the temperature in the chip-forming zone using artificial intelligence techniques. Neural Network World 20(2):171
36. Kara F, Aslantaş K, Çiçek A (2016) Prediction of cutting temperature in orthogonal machining of AISI 316L using artificial neural network. Appl Soft Comput 38:64–74
37. Korkut I, Acır A, Boy M (2011) Application of regression and artificial neural network analysis in modelling of tool–chip interface temperature in machining. Expert Syst Appl 38(9):11651–11656
38. DeChiffre L (1981) Lubrication in cutting—critical review and experiments with restricted contact tools. Asle. Transactions 24(3): 340–344
39. Debnath S, Reddy MM, Yi QS (2014) Environmental friendly cutting fluids and cooling techniques in machining: a review. J Clean Prod 83:33–47
40. Allen DM (1974) The relationship between variable selection and data agumentation and a method for prediction. Technometrics 16(1):125–127
41. Saglam H, Yaldiz S, Unsacar F (2007) The effect of tool geometry and cutting speed on main cutting force and tool tip temperature. Mater Des 28(1):101–111
42. Myers RH, Montgomery DC, Anderson-Cook CM (2016) Response surface methodology: process and product optimization using designed experiments. John Wiley & Sons, New York
43. Box GE, Draper NR (1987) Empirical model-building and response surfaces, vol 424. Wiley, New York
44. Kamruzzaman M, Dhar N (2009) The influence of high pressure coolant on temperature tool wear and surface finish in turning 17CrNiMo6 and 42CrMo4 steels. J Eng Appl Sci 4(6):93–103
45. Mia M, Khan MA, Rahman SS, Dhar NR (2016) Mono-objective and multi-objective optimization of performance parameters in high pressure coolant assisted turning of Ti-6Al-4V. Int J Adv Manuf Technol:1–10. doi:10.1007/s00170-016-9372-z
46. Hornik K, Stinchcombe M, White H (1989) Multilayer feedforward networks are universal approximators. Neural Netw 2(5):359–366
47. Beale MH, Hagan MT, Demuth HB (2010) Neural network toolbox 7. User's Guide, MathWorks
48. Mia M, Dhar NR (2016) Prediction of surface roughness in hard turning under high pressure coolant using artificial neural network. Measurement 92:464–474
49. MacKay DJ (1992) A practical Bayesian framework for backpropagation networks. Neural Comput 4(3):448–472
50. Foresee FD, Hagan MT (1997) Gauss-Newton approximation to Bayesian learning. In: Neural Networks, 1997, International Conference on. IEEE:1930–1935
51. Haykin SS, Haykin SS, Haykin SS, Haykin SS (2009) Neural networks and learning machines, vol 3. Pearson Education Upper Saddle River
52. Mia M, Dhar NR (2016) Response surface and neural network based predictive models of cutting temperature in hard turning. J Adv Res
53. Groover MP (2012) Fundamentals of modern manufacturing: materials, processes, and systems, 5th edn. Wiley Global Education
54. Trent EM, Wright PK (2000) Metal cutting. Butterworth-Heinemann
55. Kamruzzaman M, Dhar N Performance evaluation of carbide inserts in turning C-60 steel and 42crmo4 steel under high-pressure coolant (Hpc) condition
56. da Silva RB, Machado ÁR, Ezugwu EO, Bonney J, Sales WF (2013) Tool life and wear mechanisms in high speed machining of Ti–6Al–4V alloy with PCD tools under various coolant pressures. J Mater Process Technol 213(8):1459–1464